BBA - Molecular and Cell Biology of Lipids 1870 (2025) 159636

Contents lists available at ScienceDirect

BBA - Molecular and Cell Biology of Lipids

journal homepage: www.elsevier.com/locate/bbalip

Rapamycin induced autophagy enhances lipid breakdown and ameliorates lipotoxicity in Atlantic salmon cells

Kanchan Phadwal [a,*], Jennifer Haggarty [b,1], Dominic Kurian [a,1], Judit Aguilar Martí [a], Jianxuan Sun [a], Ross D. Houston [c], Mónica B. Betancor [d], Vicky E. MacRae [a,e], Phillip D. Whitfield [f], Daniel J. Macqueen [a]

[a] The Roslin Institute and Royal (Dick) School of Veterinary Studies, The University of Edinburgh, Midlothian, UK
[b] Shared Research Facilities, College of Medical, Veterinary and Life Sciences, University of Glasgow, Glasgow G12 8QQ, UK
[c] Benchmark Genetics, Edinburgh Technopole, Edinburgh, UK
[d] Institute of Aquaculture, Faculty of Natural Sciences, University of Stirling, Stirling, UK
[e] School of Life Sciences, Faculty of Science and Engineering, Anglia Ruskin University, Cambridge, UK
[f] Glasgow Polyomics and Institute of Infection, Immunity and Inflammation, College of Medical, Veterinary and Life Sciences, University of Glasgow, Glasgow, UK

ARTICLE INFO

Keywords:
Autophagy
SHK-1
Lipid droplets
Lipidomics
Proteomics
TAGs
Lipotoxicity

ABSTRACT

Autophagy is a highly conserved cellular recycling process essential for homeostasis in all eukaryotic cells. Lipid accumulation and its regulation by autophagy are key areas of research for understanding metabolic disorders in human and model mammals. However, the role of autophagy in lipid regulation remains poorly characterized in non-model fish species of importance to food production, which could be important for managing health and welfare in aquaculture. Addressing this knowledge gap, we investigate the role of autophagy in lipid regulation using a macrophage-like cell line (SHK-1) from Atlantic salmon (*Salmo salar* L.), the world's most commercially valuable farmed finfish. Multiple lines of experimental evidence reveal that the autophagic pathway responsible for lipid droplet breakdown is conserved in Atlantic salmon cells. We employed global lipidomics and proteomics analyses on SHK-1 cells subjected to lipid overload, followed by treatment with rapamycin to induce autophagy. This revealed that activating autophagy via rapamycin enhances storage of unsaturated triacylglycerols and suppresses key lipogenic proteins, including fatty acid elongase 6, fatty acid binding protein 2 and acid sphingomyelinase. Moreover, fatty acid elongase 6 and fatty acid binding protein 2 were identified as possible cargo for autophagosomes, suggesting a critical role for autophagy in lipid metabolism in fish. Together, this study establishes a novel model of lipotoxicity and advances understanding of lipid autophagy in fish cells, with significant implications for addressing fish health issues in aquaculture.

1. Introduction

Macroautophagy, hereafter referred to as autophagy, is a key cellular recycling mechanism responsible for the degradation of misfolded proteins, damaged organelles, pathogens, and other cellular components in all eukaryotic cells [1]. This process involves the formation of double-membraned autophagosomes, which fuse with lysosomes to form autolysosomes, where the cargo is broken down by lysosomal enzymes and recycled back into the cytoplasm [2]. In addition to the mentioned cargos, lipids stored as lipid droplets (LDs) are degraded through a selective form of autophagy called lipophagy [3]. Excess lipids, if not degraded or stored in LDs, can block autophagic flux, leading to further lipid accumulation and lipotoxicity [4–6]. Lipotoxicity results from the build-up of diacylglycerols and ceramides (CERs) within LDs and other non-adipose tissue [7]. CERs can be further metabolized into complex sphingolipids such as sphingomyelins (SMs), or vice versa [8]. Lipid-induced lipotoxicity is a key contributor to metabolic disorders in mammals, including insulin resistance, myosteatosis, cardiac pathologies, and non-alcoholic fatty liver disease (NAFLD) [9–11].

Atlantic salmon (*Salmo salar* L.) is the most commercially valuable farmed fish globally and an important source of high-quality protein and omega-3 fatty acids, supporting food production and representing the most advanced aquaculture sector [12]. Sustainable salmon aquaculture

* Corresponding author.
E-mail address: Kanchan.phadwal@roslin.ed.ac.uk (K. Phadwal).
[1] Equal contribution.

https://doi.org/10.1016/j.bbalip.2025.159636
Received 18 December 2024; Received in revised form 22 April 2025; Accepted 15 May 2025
Available online 17 May 2025

Abbreviations

LDs	Lipid droplets
CERs	ceramides
SMs	sphingomyelins
SHK-1	salmon head kidney cell line
RAPA	Rapamycin
MRT	MRT68921
LC3	microtubule-associated light chain 3
Plin3	Perilipin 3
TAG	triacylglycerol
Elovl6	fatty acid elongase 6
ASM	acid sphingomyelinase
SD	Standard Deviation

is challenged by a range of issues that are negatively impacting fish health and welfare, including infectious diseases caused by diverse pathogens and parasites [13]. Atlantic salmon health is also thought to be impacted by recent changes in farmed fish diets that are more environmentally sustainable and cost-effective, increasingly replacing protein and oils traditionally derived from marine sources, with those from plants [14]. Vegetable oils have more short chain (< C20) n-6 polyunsaturated fatty acids than fish oil, and reduced n-3 long-chain chain polyunsaturated fatty acids, which changes the n-3/n-6 ratio and promotes adipogenesis by lipid deposition in liver, visceral adipocytes and muscle, while causing lipotoxicity and inflammation [15,16]. In Atlantic salmon, as observed in mice [17,18], diets enriched in vegetable oils have been shown to increase adiposity [15], which may lead to lipotoxicity. In addition to having negative impacts on fish health, this is likely to negatively impact human consumers of salmon. In this respect, mice showed an increase in lipotoxic hepatic oxylipins and CERs, as well as increased insulin resistance, after consuming farmed Atlantic salmon fed a vegetable oil-enriched diet [19,20]. Oxylipins are oxidized derivatives of polyunsaturated fatty acids, while CERs are bioactive lipids involved in cell signalling, and both are associated with metabolic disorders, liver disease like NAFLD, and inflammation when present in excessive amounts [21,22].

The role of autophagy in regulating lipid accumulation and breakdown remains unexplored in Atlantic salmon, but represents an important target to better understand and improve the health and welfare of farmed fish. In this study, we used a macrophage-like cell line derived from the head kidney (SHK-1, [23]) as an established in vitro model to test the hypothesis that autophagy regulates lipid accumulation and breakdown in Atlantic salmon. We demonstrate that LDs colocalize with key lipophagy markers in Atlantic salmon cells, Moreover, omics provides evidence of lipotoxicity that strongly mirrors human NAFLD in lipid-treated SHK-1 cells; this was ameliorated by autophagy induction, which enhanced unsaturated triacylglycerol (TAG) storage and suppressed lipogenic protein expression. We also show that key lipogenic proteins are cargo for autophagosomes, suggesting that autophagy plays a pivotal role in regulating enzymes involved in altering fatty acid composition and lipid metabolism. The suppression of acid sphingomyelinase activity following autophagy induction further highlights the potential role of autophagy in modulating SM metabolism. Finally, we discuss the implications of our findings for understanding mechanisms of lipid metabolism in farmed fish and the potential to promote health in salmon aquaculture.

2. Methods

2.1. Cell culture and experimental setup

The SHK-1 cell line (ATCC 97111106) [23] was cultured in complete L15 media (10 % FCS, 5 % Penicillin/Streptomycin and 400 μL beta Mercaptoethanol). Cells were incubated in the dark, in a 19 °C incubator with CO_2. Lipid overload was achieved by treating the cells with 2.5 % lipid mixture [24] (Sigma, L0288), which contains non-animal derived fatty acids (2 μg/mL arachidonic and 10 μg/mL each linoleic, linolenic, myristic, oleic, palmitic and stearic acid), 0.22 mg/mL cholesterol from New Zealand sheep's wool, 2.2 mg/mL Tween-80, 70 μg/mL tocopherol acetate and 100 mg/mL Pluronic F-68 solubilized in cell culture water. Autophagy was induced by treating SHK-1 cells with 1 μM rapamycin (RAPA) (APExBIO, A8167). Autophagic flux was blocked using 10 nM Bafilomycin-A (Baf-A) (MERK, B1793), while autophagy was blocked using 500 nM MRT68921 (MRT) (APExBIO, B6174). LD staining with (boron-dipyrromethene) BODIPY, LC3 and Perilipin 3 (Plin3) done with cells treated for a period between 24 and 72 h, with remaining experiments performed using cells treated for 72 h. DMSO concentration was kept at 0.01 % for all experiments. A schematic diagram summarising the experiments is shown in Fig. 1A.

2.2. Lipid droplet and immunofluorescence staining

LDs were stained with 1 μM BODIPY 493/503 (D3922). BODIPY 493/503 staining was combined with rabbit polyclonal LC3 (1:300, PM036) and Plin3 (1:300, Abcam, ab47638) for immunofluorescence (IF). Prior to IF, SHK-1 cells were fixed in 4 % paraformaldehyde for 20 mins at room temperature and then blocked and permeabilised in blocking buffer (0.2 M Glycine, 0.1 mg/mL saponin and 30 mg/mL BSA in PBS) for 1 h at room temperature. The cells were then incubated with primary antibodies overnight. The cells were then washed three times with PBS and incubated with 1:500 secondary antibody, donkey anti Rabbit 647 (Bio Legend, 406414) for 1 h at room temperature. After 3 washes, cells were stained with 1:10,000 Hoechst for 1–3 min and mounted on glass slides with ProLong glass antifade mountant (Invitrogen, P36982).

Using the same methodology, but with an additional blocking step (using 5 % goat serum for 45 mins), SHK-1 cells were stained with a combination of 1:250, rat monoclonal LAMP1–546 (SC-19992) and rabbit polyclonal ASM (DF-13384), rabbit polyclonal Elovl-6 (DF-4039) on its own, or goat polyclonal Fabp2 (A84334) on its own. All the experiments were visualised on a LSM880 laser scanning microscope produced (Zeiss) with image analysis performed using Fiji [25].

2.3. Transmission electron microscopy

SHK-1 cells were detached using Trypsin/EDTA, centrifuged, and washed twice with PBS. The cells were then fixed overnight in 2.5 % glutaraldehyde and 4 % paraformaldehyde in 0.1 M cacodylate buffer. After fixation, they were washed in 0.1 M cacodylate buffer and post-fixed with 1 % osmium tetroxide and 0.8 potassium ferrocyanide in water for 60 min. Samples were washed in 0.1 M cacodylate buffer, followed by en bloc staining with 0.5 % uranyl acetate for 30 min. The samples were then dehydrated through a graded acetone series (50 %, 70 %, 90 %, and 100 %, for 10 min each). They were then embedded in TAAB 812 resin.

Semi-thin sections were cut using a ultramicrotome (Leica, Germany), stained with toluidine blue, and examined under a light microscope to identify suitable areas. Ultrathin sections (60 nm) were then cut, stained with uranyl acetate and imaged using a JEOL 1400 Plus transmission electron microscope (Jeol, Japan).

2.4. Mitotracker staining, reactive oxygen species measurement and cell proliferation assays

SHK-1 cells were seeded in 96 well plates at a density of 20,000 cells/well and were treated for 72 h as described in the section “Cell culture and experimental setup”, except that Bafilomycin-A1 and MRT were not used for these experiments.

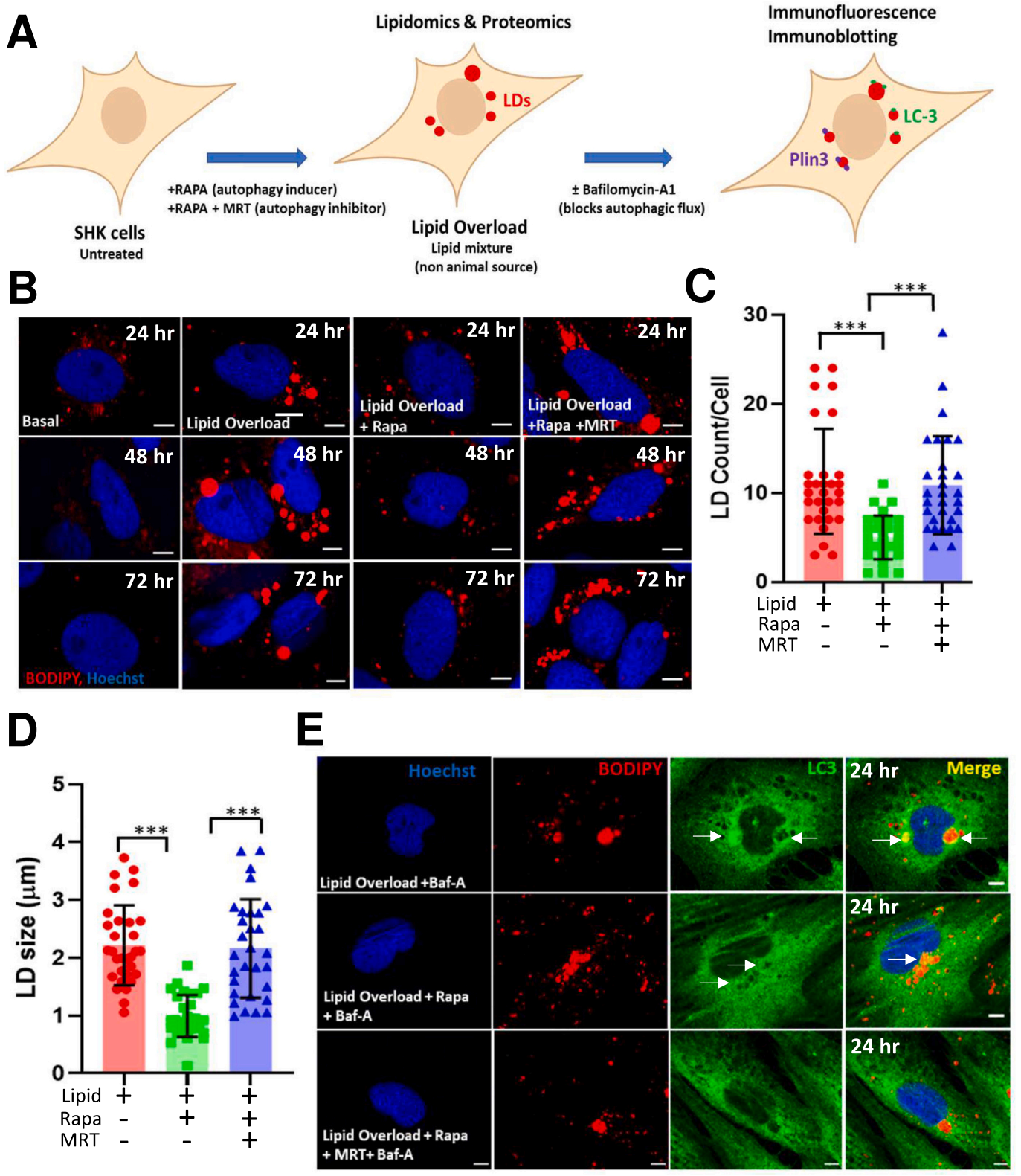

Fig. 1. Lipid overload inhibits LD breakdown by blocking autophagic flux in SHK-1 cells. A. Schematic overview of experiments performed in this study. B. LD count and size measurements in SHK-1 cells following 24, 48 and 72 h treatments under basal, lipid overload, lipid overload with RAPA, and lipid overload with RAPA+MRT. C. Quantification of LD numbers at 48 h (30 cells counted from 3 independent experiments). D. Quantification of LD size at 48 h (30 cells counted from 3 independent experiments). E. Representative confocal images showing the colocalisation of LC3 (green puncta) with LDs stained with BOPIPY (red). Baf-A was added to all treatments to block the autophagic. Scale bar = 10 μm, $n = 3$. Data shown as mean +/− SD, ***$p < 0.001$. (For interpretation of the references to colour in this figure legend, the reader is referred to the web version of this article.)

SHK-1 cells were then stained with 100 nM MitoTracker Red CMXRos (Invitrogen, Waltham, MA, USA) in the L15 complete media for 30 min at 20 °C incubator without CO_2. The 96 well plate was then read for the fluorescence endpoint at excitation/emission at 560 nm/599 nm. using a Cytation 3 spectrophotometer.

ROS production in SHK-1 cells was determined using a commercially available DCFDA/H2DCFDA - Cellular ROS Assay Kit (Abcam). The fluorescence end point was measured at excitation/emission at 485 nm/535 nm.

Cell proliferation was measured using CyQUANT™ NF Cell Proliferation Assay Kit (C35007). The fluorescence end point was measured at excitation/emission at 485 nm/535 nm.

2.5. Sphingomyelinase assay

Acid Sphingomyelinase activity was assessed using an Amplite® Fluorimetric Acid Sphingomyelinase Assay *Red Fluorescence* Kit (AAT Bioquest), following the manufacturer's instructions. SHK-1 cells were cultured in 6 well tissue culture plates and treated for 72 h (Fig. 1A). Cells were then washed with cold 2× PBS and scraped into 200 μL of RIPA Lysis buffer (Thermo Scientific, 89901). The lysed cell extract was centrifuged at 12,000 RPM for 20 mins at 4 °C and the supernatant collected. 50 μL each of SM standard, test solution (i.e., cell extract) and a blank solution were added in duplicates to black bottomed 96 well plates. To this, 50 μL of SM working solution was added, and plates were incubated for 1 h at 37 °C. Next 50 μL of SM working solution was added to each well and further incubated for 1 h at room temperature. The plates were wrapped in aluminium foil to protect from light. Fluorescence was read at 540/590 nm using a BioTek Cytation 3 Cell Imaging MultiMode Microplate Reader.

2.6. Immunoblotting assays

A standard immunoblotting protocol was used for rabbit polyclonal antibodies for LC3 (1:3000, PM036), SQSTM1/p62 (1:500, Ab 264313), ATGL (1:500, Proteintech, 55190–1-AP), and MGL (1:500, Proteintech, 20494–1-AP). Gel quantification was performed using Fiji software. All the blots were normalised against estimated total protein concentration on a per sample basis.

2.7. Lipidomics

Lipids were extracted from SHK-1 cells according to the method described by Folch et al [27]. Samples were extracted in a 2/1 (*v*/v) chloroform/methanol solution. The samples were left at 4 °C for 1 h then partitioned by addition of 0.1 M KCl. The mixture was centrifuged to facilitate phase separation. The lower chloroform layer was evaporated to dryness under a steady flow of nitrogen gas and reconstituted in methanol containing 5 mM ammonium formate.

Following extraction, lipids were analysed by liquid chromatography-mass spectrometry (LC-MS) using a Thermo Exactive Orbitrap mass spectrometer equipped with a heated electrospray ionization (HESI) probe and interfaced with a Dionex UltiMate 3000 RSLC system (Thermo Fisher Scientific, Hemel Hempstead, UK). Samples (10 μL) were injected onto a Thermo Hypersil Gold C18 column (2.1 mm × 100 mm; 1.9 μm) maintained at 50 °C. *mobile* phase A consisted of water containing 10 mM ammonium formate and 0.1 % (*v*/v) formic acid. Mobile phase B consisted of a 90/10 (v/v) mixture of isopropanol: acetonitrile containing 10 mM ammonium formate and 0.1 % (v/v) formic acid. The LC gradient, maintained at a flow rate of 400 μL/min, was as follows; a starting condition of 65 % mobile phase A, 35 % mobile phase B. Mobile phase B increased from 35 to 65 % over 4 min, followed by 65 % to 100 % over 15 min, with a hold for 2 min before re-equilibration to the starting conditions over 6 min. All samples were analysed in positive and negative ionization modes over the mass-to-charge ratio (*m*/*z*) range of 250 to 2,000 at a resolution of 100,000. The data was processed with Progenesis QI v2.4 software (Non-linear Dynamics). Relative fold quantification was performed using all ion normalization, with outputs limited to ion signals with intensities that showed 1.5-fold (or greater) difference between the study conditions and displayed statistical significance ($p \leq 0.05$). This approach was performed for data acquired in both positive and negative ionization modes. Significant features were then identified using both the Lipid Maps and HMDB databases with a mass error tolerance of 5 ppm. Confident annotations were allocated based on expected adducts for each lipid class versus the detected adducts.

For further network analysis of lipid classes, we used LINEX^2, a lipid network explorer that integrates lipid-metabolic reactions from public databases to generate a dataset-specific lipid interaction network, revealing candidate enzymes involved in these networks [28]. For this analysis, we used all confident lipid IDs (i.e., >1.5-fold change) from the lipidomics analysis (Supplementary data 1). Lipid data files and sample data files with the group names were uploaded on the LINEX^2 software. The lipid IDs were converted to LipidLynxX Nomenclature and checked against inbuilt *Danio rerio* Rhea and Reactome Databases. The *p* value was set to 0.05 to visualise fold change between lipid overload and RAPA-treated SHK-1 samples.

2.8. Proteomics

Cells were washed and resuspended in an extraction buffer containing 5 % SDS, 50 mM Triethyl Ammonium Bicarbonate (TEAB), pH 8.5 at sample to buffer ratio of 1:10 (*w*/*v*) and homogenized using Precellys homogenizer at 5,000 g for 20 s in a ceramic beads vial (Precellys Lysing Kit, Tissue homogenizing CK mix). The extracts were centrifuged for 10 mins at 16,000 g and the supernatant sonicated for 10 cycles (30 s on, 30 s off per cycle) on a Bioruptor Pico Sonicator (Diagenode). After sonication, samples were centrifuged (16,000 ×*g* for 10 mins), before the supernatant was collected and a bicinchoninic acid assay was performed to assess protein concentration.

The protein samples were digested on the S-Trap micro column (Protifi, USA) following the manufacturer's protocol with minor modifications. Briefly, 20 μg protein in extraction buffer was reduced and alkylated using 10 mM dithiothreitol and 40 mM iodoacetamide respectively, at 45 °C for 15 m. Alkylation was stopped by adding phosphoric acid to a final concentration of 2.5 %. The protein solution was diluted six-fold with binding buffer (90 % *v*/v, Methanol in 100 mM TEAB), vortexed gently and loaded into an S-Trap micro column. After centrifugation at 4,000 *g* for 1 m, the column was washed three times with 150 μL binding buffer. Proteolytic digestion was carried out by adding 20 μL of digestion buffer containing 1 μg trypsin in 50 mM TEAB. The column was incubated at 47 °C for 2 h. Digested peptides were eluted using 4 μL of three buffers consecutively: (i) 50 mM TEAB, (ii) 0.2 % (*v*/v) Formic acid in H_2O, and (iii) 50 % (v/v) acetonitrile. Eluted peptides were pooled and cleaned up using C18 stage tips and dried under vacuum.

Purified peptides were separated over a 70 m gradient on an Aurora-25 cm column (IonOpticks Australia) using an UltiMate RSLCnano LC System (ThermoFisher Scientific) coupled to a timsTOF FleX mass spectrometer via a Captivespray ionization source. The gradient was delivered at a flow rate of 200 nL/mins and the column temperature was set at 50 °C. The TIMS elution voltage was linearly calibrated to obtain 1/K0 ratios using three ions from the ESI-L Tuning Mix (Agilent, Santa Clara, CA, USA) (*m*/*z* 622, 922, 1222) using timsControl (Bruker). For Data Dependent Acquisition (DDA) - Parallel Accumulation-Serial Fragmentation (PASEF) acquisition, the full scans were recorded from 100 to 1700 m/z spanning from 1.45 to 0.65 Vs/cm2 in the mobility (1/K0) dimension. Up to 10 PASEF MS/MS frames were performed on ion-mobility separated precursors, excluding singly charged ions which are fully segregated in the mobility dimension, with a threshold and target intensity of 1750 and 14,500 counts, respectively. The collision energy was ramped linearly from 59 eV at 1/k0 = 1.6 to 20 eV at 1/k0 = 0.6.

Raw mass spectral data was processed using PEAKS Studio X-Pro Software (Bioinformatics LTD) [29], with protein searches conducted against the Ensembl 113 annotation for Atlantic salmon (https://www.ensembl.org/Salmo_salar/Info/Index), which contains 146,172 unique amino acid sequences (derived from 47,205 coding genes). MS1 precursor mass tolerance was set to 20 ppm, and the MS2 fragment ion tolerance was 0.06 Da. The search parameters specified fully tryptic digestion, allowing for one missed cleavage. Cysteine was treated as a fixed modification with a mass addition of [+57.02], while methionine oxidation and deamination of asparagine and glutamine were set as variable modifications. Quantitative LFQ analysis was performed using default settings, with optional identification transfer enabled.

2.9. Quantification of confocal images using Fiji

The confocal images in Figs. 1B, 3A, 5A and 7A were analysed quantitatively using ImageJ-win64 (Fiji app) [25]. For LD size, the diameter of each LD was measured with the freehand line tool. For LD counts and ASM in the extracellular matrix, the multipoint tool was used to count LDs and ASM within each cell and across the entire microscopic field. Colocalization of Plin3 and BODIPY was assessed with the Colocalisation Finder plugin, enabling precise analysis of overlapping signals. Fluorescent intensity for Elovl6 and Fabp2 was measured using mean intensity feature in the respective channel.

2.10. Quantitative PCR (qPCR)

Primers for real-time qPCR expression analyses of target genes (encoding Elovl6 and Fabp2 proteins) were designed using Primer3 [26] to distinguish closely related paralogous sequences retained from whole genome duplication events in salmonid evolution [12]. Gene sequences were retrieved from the Atlantic salmon reference genome (Ssal_v3.1; GCA_905237065.2) using the Ensembl Genome Browser (Release 113). With the aim of achieving paralog-specific amplification, primers were positioned within regions of high sequence divergence, identified through multiple sequence alignment, particularly at the 3′ of primer sequences. Details of all primer sequences used, including database accession numbers is provided in Supplementary Table 1. SHK-1 cells were cultured in 6 well tissue culture plates. On confluency, they were either left untreated or treated with lipid overload, lipid overload and rapamycin and lipid overload and rapamycin and MRT (as described above). RNA was extracted using a Qiagen-rneasy-mini-kit then reverse transcribed before target cDNA quantification using a Luna® Universal One-Step RT-qPCR Kit (NEW ENGLAND BIOLABS (UK) LTD, E3005L). Reactions were performed with an CFX Opus Real-Time PCR System (Bio-Rad) with 1 cycle of 10 min at 55 °C (Reverse Transcription), followed by initial denaturation for 1 min at 95 °C, denaturation for 10s at 95 °C and extension for 40 cycles of 30 s at 60 °C. Cycle threshold (Cq) values were obtained with CFX Maestro Software (Bio-Rad) and relative gene expression values were calculated using GenEX™ Professional software (MultiID). All the experimental genes were normalised in GeneEX to Cq values using two reference genes, *rps20* and *18sRNA*. Each gene analysed showed a single peak in its melting curve.

2.11. Statistics and reproducibility

Data are presented as mean ± SD in bar graphs. Statistical significance was determined using two-tailed Student's *t*-test via GraphPad Prism software (Version 8.1.1), with *p* values indicated in the corresponding figures. $p < 0.05$ was considered statistically significant for most of the experiments except for proteomics analysis where $p < 0.01$ (adjusted) was considered statistically significant. The exact sample size (*n*) for each experiment is presented in the figure legends. All experiments were performed at least three times independently, yielding consistent results. Statistical analyses from confocal microscopy excluded dead cells showing abnormal nuclear staining, i.e., nuclear condensation.

3. Results

3.1. Lipid overload prevents LD breakdown by blocking autophagic flux in SHK-1 cells

We first tested whether LDs generated by lipid overload in SHK-1 cells are regulated by autophagy across a time course, taking samples at 24, 48 and 72 h following treatment with a 2.5 % lipid mixture. To enhance the autophagic flux we added 1 μM RAPA [30] and to block autophagosome formation/maturation we treated the cells with 500 nm MRT68921 (MRT) [31]. Firstly, we checked endogenous levels of LD in SHK-1 cells untreated with a lipid mixture, observing negligible BODIPY staining (Fig. 1B). In comparison, SHK-1 cells treated solely with lipid mixture showed several large circular LDs, mostly in close proximity to the nucleus (Fig. 1B). Blocking the formation of autophagosomes with MRT in lipid overload treated cells resulted in significantly increased and aggregated LDs (Supplementary Fig. 1) suggesting a direct role of autophagy in LD breakdown. Autophagy induction via RAPA treatment resulted in significantly reduced LD number and size (Fig. 1B-D). However, further treatment with RAPA+MRT led to large LDs at all timepoints, which showed clumping at 72 h (Fig. 1B). To avoid clumped LDs that were present at 72 h, we quantified differences in size and number of LDs across treatment at 48 h (Fig. 1C-D). These results indicate that autophagy induction acts to breakdown LDs, but this effect is ablated by blocking autophagosome formation and maturation.

To further validate the above results, it was important to ask whether LDs colocalise with punctate LC3, the marker for mature autophagosomes, which we achieved by blocking autophagic flux using 10 nM Baf-A [32]. Baf-A interrupts autophagic flux by inhibiting V-ATPase-dependent autophagosome-lysosome fusion [33]. This approach aids in visualisation of LD cargo within autolysosomes, the autophagosome-lysosome fusion vesicle. While we imaged SHK-1 cells at all tested time points, LD-LC3 colocalisation was only observed 24 h post lipid treatment (Fig. 1E). We specifically observed colocalisation of dense LC3 around large LDs within close proximity to the nucleus (Fig. 1E). After RAPA treatment, LC3 puncta were observed around several smaller LDs spread across the cytoplasm and also within close proximity of the nucleus (Fig. 1E). The same colocalisation appeared reduced on the largest LDs following MRT treatment (Fig. 1E), suggesting LC3 binds to LDs in SHK-1 cells.

To further support our findings, we used transmission electron microscopy (TEM), the gold standard for visualizing autophagosomes, under the same treatment conditions. We observed LDs engulfed in autophagosomes in rapamycin-treated cells (Fig. 2B-C). However, cells under lipid overload and MRT treatment failed to form complete autophagosomes, though fragments of lipid bilayers were seen at the periphery (Fig. 2A & D).

We also investigated whether lipid overload and subsequent rapamycin treatment affected mitochondrial health, apoptosis, reactive oxygen species (ROS), and cellular proliferation. TEM images showed no major morphological changes in mitochondria with or without 24 h of lipid treatment, though mitochondria appeared swollen under lipid overload, possibly indicating damage (Supplementary Fig. 2A-B). Additionally, peridroplet mitochondria (mitochondria in direct contact with LD) [34] were observed in cells treated with lipid overload and following further treatment with rapamycin, and MRT. However, lipid overload with rapamycin-treated cells displayed mitochondrial clustering around LDs (Supplementary Fig. 2C-E).

To assess mitochondrial membrane potential, we stained SHK-1 cells with MitoTracker Red CMXROS, a cell-permeable dye that accumulates in healthy mitochondria. Cells treated with lipid overload for 72 h showed a significant drop in membrane potential compared to control and rapamycin-treated cells (Supplementary Fig. 2F), suggesting lipid overload may impair mitochondrial function. No signs of apoptosis

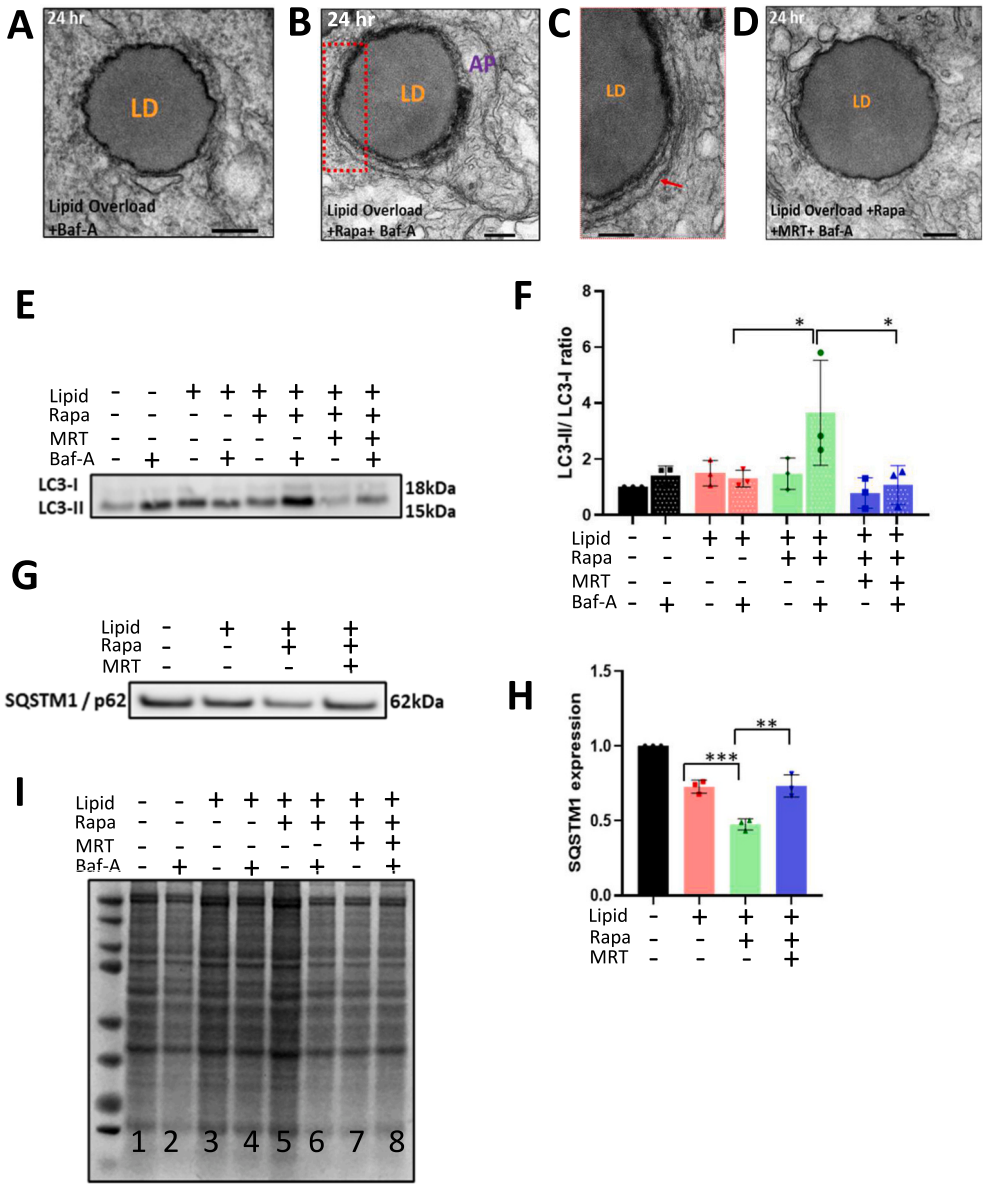

Fig. 2. Rapamycin treatment shows lipid droplets packed inside autophagosomes and enhanced autophagic flux in Atlantic salmon SHK-1 cells under lipid overload. SHK-1 cells were treated for 24 h with lipid overload, lipid overload with RAPA, and lipid overload with RAPA+MRT and the autophagic flux was blocked with Baf-An under all treatments. A. LD were seen with peripheral rudimentary lipid bilayers under the lipid overload treatment. B. LD were seen surrounded by an autophagosome (AP) with further rapamycin treatment. C. Zoomed-in lipid bilayers of an autophagic vesicle. D. LD was seen with peripheral rudimentary lipid bilayers under lipid the overload treatment with rapamycin and MRT. Scale bars are as shown in the images. E. Representative immunoblot and F. Immunoblot quantification showing LC3 abundance in SHK-1 cells after 72 h treatment with no lipid overload, lipid overload, lipid overload with RAPA, and lipid overload with RAPA and MRT treatments, with and without Baf-A ($n = 3$). G. Representative immunoblot and H. Immunoblot quantification showing SQSTM1/p62 abundance in SHK-1 cells after 72 h treatment with no lipid overload, lipid overload, lipid overload with RAPA, and lipid overload with RAPA and MRT treatments. I. Total protein blot stained with simply blue safe stain for protein abundance quantification. Lanes 1, 3, 5 and 7 were used to quantify SQSTM1/p62 in blot G. Data shown as mean +/− SD, * $p < 0.05$; ** $p < 0.01$. (For interpretation of the references to colour in this figure legend, the reader is referred to the web version of this article.)

(fragmented nuclei) were observed under lipid overload. Also, ROS production and cellular proliferation remained unchanged after 72 h of treatment (Supplementary Fig. 3A-B).

To further validate that RAPA was inducing autophagic flux, we measured protein abundance levels of LC3 (with and without addition of Baf-A to all the treatments) and SQSTM1/p62 without addition of Baf-A. LC3 exists as the non-lipidated form LC3-I in the cytoplasm, after lipidation by E1, E2, and E3-like enzymes, respectively (ATG7, ATG3, and a complex consisting of ATG12-ATG5 and ATG16L1), conjugating the cytosolic LC3-I protein to phosphatidylethanolamine to form LC3-II [35]. A combined increase in expression of LC3-II with reduction in SQSTM1/p62 (an autophagy adaptor that gets co-degraded with the cargo) levels is considered to arise from increased autophagic flux [36]. In SHK-1 cells, we observed increased LC3-II expression following RAPA treatment compared to cells solely treated with lipid overload or with additional MRT treatment in the presence of Baf-A (Fig. 2E-F). RAPA treatment reduced SQSTM1/p62 expression, while both lipid overload and MRT treatments enhanced SQSTM1/p62 expression, suggesting a block in autophagic flux on lipid treatment (Fig. 2G-H). The total protein levels used for normalization are provided in Fig. 2I.

3.2. RAPA enhances lipid droplet breakdown via perilipin 3 and upregulation of key lipases

Our next question was whether LDs in SHK-1 cells colocalise to Plin3, a protein that coats LDs and acts as a key marker for lipophagy. Plin3 is required for docking autophagy machinery to LDs and its silencing blocks LD-associated LC3-II autophagic flux [37]. LD-Plin3 co-localisation was observed at all three time points after blocking autophagic flux with Baf-A. Blockage of autophagic flux led to accumulation of more small LDs in RAPA-treated cells compared to the lipid overload and MRT treated cells, which showed bigger LDs (Fig. 3A-B, 72 h data shown). The small LDs observed in RAPA-treated cells were further surrounded with more Plin3 compared to LDs in lipid overload (Fig. 3A-B). Plin3 was strongly associated with small LDs, as assessed by Pearson's coefficient (Fig. 3C), with large LDs showing a more limited association with Plin3, especially in cells with lipid overload. These results clearly suggest a role for Plin3 in RAPA-induced LD breakdown in SHK-1 cells.

We further assessed the expression of key lipase proteins, i.e., adipose triglyceride lipase (ATGL) [38] and monoglyceride lipase (MGL) [39] in SHK-1 cells treated with lipid overload, RAPA and MRT. The abundance of both the proteins was reduced under both the lipid overload and when the autophagosome formation was blocked with MRT treatment for 72 h (Fig. 3D-F). Together, these results suggest that SHK-1 cells have all the key molecules required for LD breakdown via autophagy, which are inhibited by lipid overload, a process that can be experimentally reversed by enhancing autophagic flux.

3.3. Autophagy supresses bioactive ceramides and upregulates PUFA-TAGs

To gain a global perspective on the role of lipid autophagy in SHK-1 cells, we examined changes in lipid pool abundance using lipidomics, following the induction of autophagy with RAPA in comparison to the lipid overload treatment (72 h post-treatments). The global lipidome of SHK-1 cells under lipid overload exhibited an increased abundance (>2-fold change) of SMs, including SM 36:0 and SM 36:1. In contrast, cells treated with RAPA showed an increased abundance (>2-fold change) of long-chain PUFA-triacylglycerols (TAGs) containing 55–60 carbons with 5–9 double bonds, alongside ion signals likely attributable to TAGs containing polyunsaturated fatty acids (Fig. 4A-B).

Lipotoxicity is associated with altered levels of CER, diacylglycerols, and SM [40–42]. SM 36:0 and SM 36:1, identified under lipid overload, have been shown to be upregulated in lipid metabolic disorders such as fatty liver, liver steatosis in NAFLD, high-fat diets, and obesity **[41,43–45]**. To further explore evidence for lipotoxicity in our data, we employed LINEX^2, a lipid network explorer that integrates lipid-metabolic reactions from public databases to generate a dataset-specific lipid interaction network (Fig. 4C), revealing candidate enzymes which may be involved in these networks [28]. The LINEX^2 network enrichment revealed two key networks, the TAG network upregulated following RAPA treatment, and the CER-SM network upregulated by the lipid overload treatment (Fig. 4C). LINEX^2 identified five candidate enzymes based on metabolite abundances between lipid overload and SHK-1 cells treated with RAPA (Fig. 4C-D). Among the predicted enzymes for the lipid overload treatment, we selected acid sphingomyelinase (ASM), which resides in lysosomes [46] and it is likely to impact or be impacted by blocked autophagic flux seen in lipid overload treatments [47,48] (Fig. 4D), for further analysis.

ASM is mainly a lysosomal lipid hydrolase, where it cleaves the sphingolipid, sphingomyelin, into CER and phosphocholine. Knockout of ASM in hepatocytes inhibits palmitic acid induced lipotoxicity [49]. ASM is also known to localise to the plasma membrane and the extracellular space [46]. We therefore asked whether lipid overload or RAPA treatment alters the localization of ASM, and if this is dependent on autophagy. We performed immunofluorescence staining for ASM and the key lysosomal marker LAMP-1 (lysosomal-associated membrane protein 1) after treating SHK-1 cells with a lipid mixture, the same lipid mixture plus RAPA, and after subsequently blocking autophagy with MRT (Fig. 1A).

Under lipid overload, ASM predominantly localized within the lysosomes (Fig. 5A). However, treatment with RAPA induced the exocytosis of ASM into the extracellular space via LAMP-1 positive vesicles (Fig. 5A, white arrows). Interestingly, when autophagy was blocked using MRT, we observed an increase in the retention of ASM within LAMP-1 positive lysosomes, particularly around the nucleus (Fig. 5A). These findings suggest that in the absence of autophagy, ASM remains confined to lysosomes, highlighting autophagy's essential role in regulating its localization (Fig. 5B). As an alternative approach, we assessed SMase activity using a fluorimetric sphingomyelinase assay in SHK-1 cells under the same experimental conditions. RAPA treatment resulted in reduced SMase activity compared to cells treated with the lipid mixture alone, while SMase activity significantly increased when autophagy was blocked with MRT (Fig. 5C). These results indicate a role for autophagy in modulating SMase activity.

3.4. Rapamycin ameliorates lipid overload mediated lipotoxicity in SHK-1 cells

To better understand the functional impacts of autophagy induction on SHK-1 cells, we performed a proteomics analysis comparing the lipid overload vs. lipid overload + RAPA treatments after 72 h (Fig. 1A). 5971 proteins were confidently detected in SHK-1 cells (Supplementary data 2). We focused on those showing changes in abundance >1.5-fold increase or < 0.5-fold decrease ($p < 0.01$) (Fig. 6A). This approach identified 20 upregulated and 3 downregulated proteins under lipid overload compared to lipid overload + RAPA. Among the 21 up-regulated proteins, one was uncharacterized. 13 of the remaining 20 Atlantic salmon proteins were orthologues of human proteins associated with fatty liver disease according to a published database [50] (Fig. 6B), along with 2 of the 3 downregulated proteins, suggesting a strong level of functional conservation across distant vertebrate species. These 16 proteins were arranged in descending order of their standardized value scores (log10 *p*-value) to represent the relative strength of functional association with fatty liver pathology in human (Fig. 6C).

3.5. Elovl6 and Fabp2 as targets for selective autophagy in SHK-1 cells

Among the proteins upregulated by lipid overload according to proteomics, we selected Elovl6 (fatty acid elongase 6) and Fabp2 (fatty acid binding protein 2) for additional validation and downstream analysis, as they had among the highest functional association scores with fatty liver pathology (Fig. 6C) and are known to have direct roles in triacylglycerol synthesis.

Elovl6 is involved in the elongation of saturated and monounsaturated fatty acids, particularly converting 12, 14 and 16 carbon fatty acids [51]. Its role in mammalian lipid metabolism has drawn significant attention in the context of metabolic diseases such as NAFLD and obesity due to its influence on lipid accumulation, inflammation, and insulin resistance [52]. Inhibiting Elovl6 activity may help prevent the conversion of palmitate to longer-chain fatty acids, thus reducing lipotoxicity and inflammasome activation, which are crucial factors in the progression of fatty liver disease [52]. We analysed changes in Elovl6 protein levels in SHK-1 cells using immunofluorescence. Our results showed an increase in Elovl6 abundance in cells treated with lipid overload and when autophagy was blocked using MRT, compared to those treated with RAPA (Fig. 7A-B). When autophagic flux was blocked with MRT and Baf-A, we observed a significant aggregation of Elovl6 in SHK-1 cells treated with lipid overload, indicating an accumulation of Elovl6 protein in the absence of autophagy (Fig. 7A-C).

Fabp2 plays a role in dietary fatty acid uptake and intracellular transport. It binds saturated long-chain fatty acids with high affinity, but has a lower affinity for unsaturated long-chain fatty acids. The

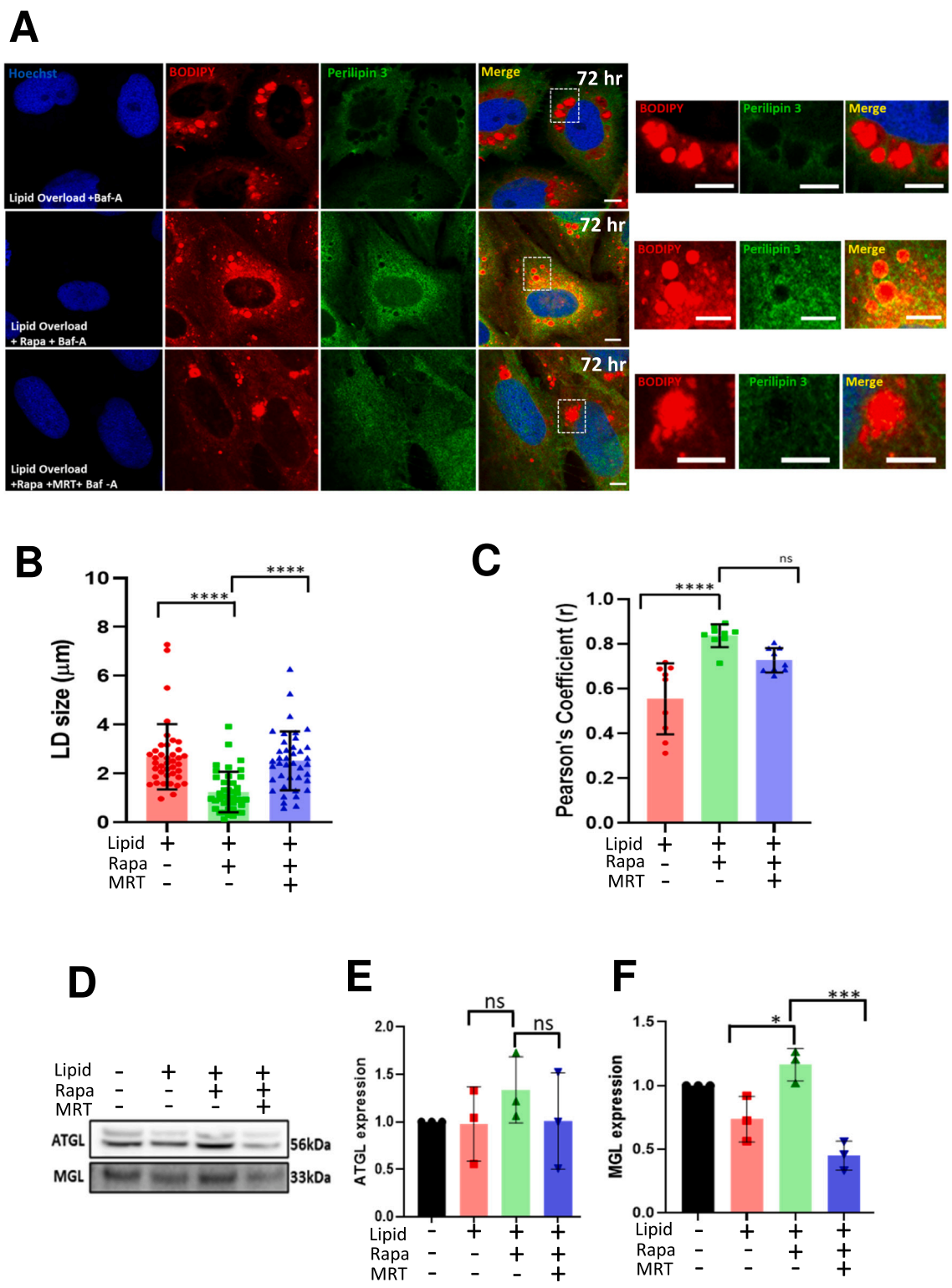

Fig. 3. Rapamycin enhances Lipid droplet breakdown via perilipin 3 and upregulation of key lipases. A. Representative confocal images showing the co-localisation of Plin3 (green puncta) with LD stained with BOPIPY (red) in SHK-1 cells after 72 h treatment with lipid overload, lipid overload with RAPA, and lipid overload with RAPA and MRT treatments. Baf-A was added to all treatments to block the autophagic flux. Zoomed-in areas in white dotted squares indicate co-localisation between perilipin 3 and LDs. Scale bar = 10 μm, n = 3, Scale bar = 5 μm for zoomed in areas. B. Quantification of lipid droplet size (40 cells were counted from 3 independent experiments). C. Quantification of co-localisation between Plin3 and lipid droplets as measured by Pearson's correlation co-efficient. D. Representative immunoblot and E-F. Immunoblot quantification showing ATGL and MGL abundance in SHK-1 cells after 72 h treatment with no lipid overload, lipid overload, lipid overload with RAPA, and lipid overload with RAPA and MRT treatments. The blots were normalised against total protein (Lanes 1, 3, 5 and 7) in Fig. 2I (n = 3). Data shown as mean +/− SD, * $p < 0.05$; *** $p < 0.001$; **** $p < 0.0001$, ns = non-significant. (For interpretation of the references to colour in this figure legend, the reader is referred to the web version of this article.)

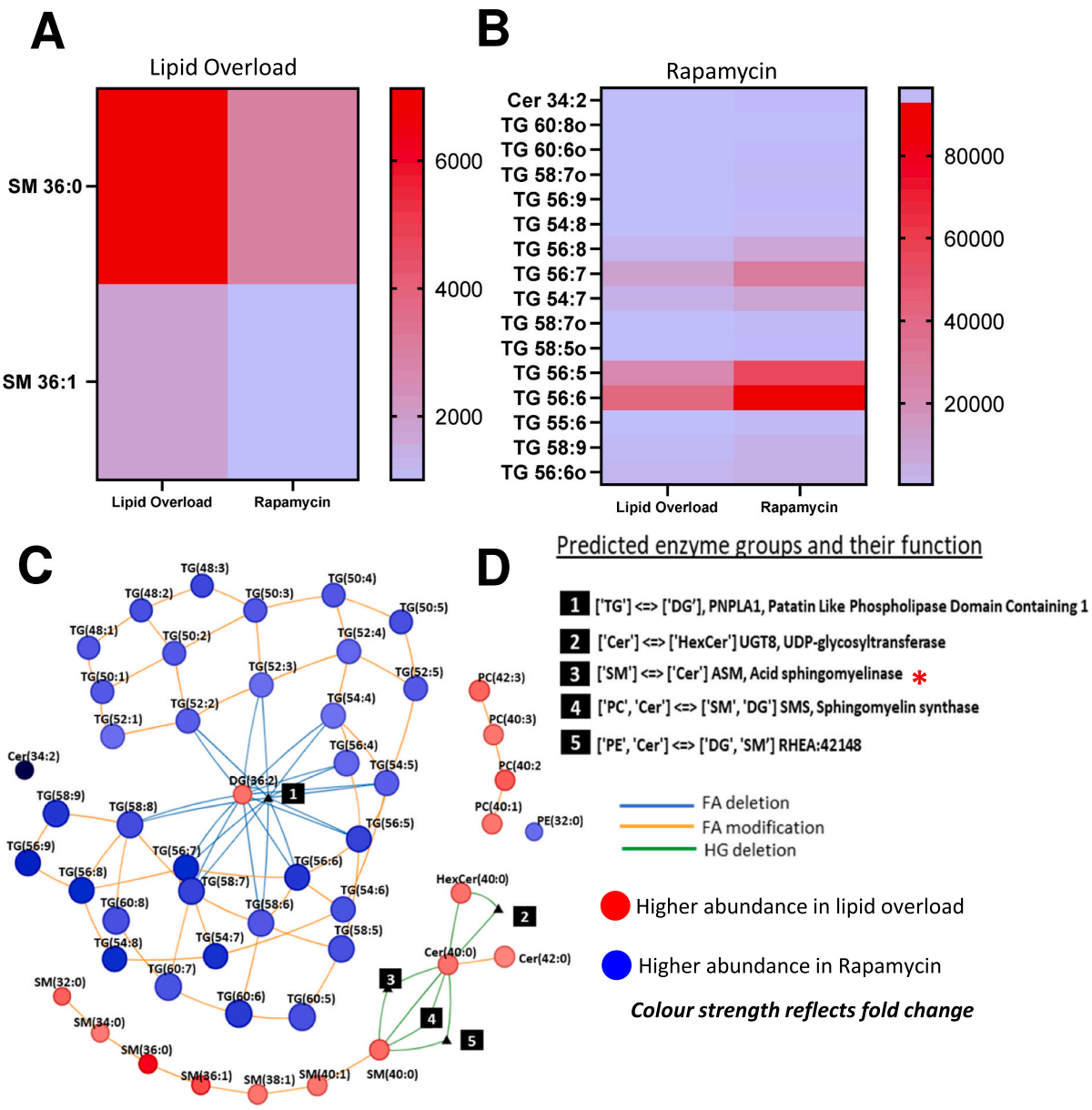

Fig. 4. Autophagy supresses bioactive ceramides and upregulates the PUFA-TAG pool. SHK-1 cells treated with lipid overload and lipid overload with RAPA treatment for 72 h were analysed for lipidome changes. A. Heat map of saturated SMs (>2 fold up-regulated) under lipid overload treatment. B. Heat map of PUFA-TAGS (>2 fold up-regulated) under lipid overload and RAPA treatments. C. LINEX^2 network enrichment analysis showing two key networks, the TAG network upregulated under RAPA treatment (blue circles) and ceramide-sphingomyelin network upregulated under lipid overload treatment (red circle) (both including lipid species showing >1.5-fold change). D. The embedded table shows five enzymes responsible for the networks shown were predicted by LINEX^2 based on metabolite abundances of SHK-1 cells following lipid overload and lipid overload with RAPA. The red asterisk indicates acid sphingomyelinase, which was further investigated. Data shown $p < 0.05$. (For interpretation of the references to colour in this figure legend, the reader is referred to the web version of this article.)

expression of Fabp2 correlates with lipid droplet storage in enterocytes [53] and has been found to increase in fish fed an oxidized fish oil diet [54]. We conducted the same experiment with Fabp2 as for Elovl6 (Fig. 7D-E). Like Elovl6, Fabp2 levels increased in cells subjected to lipid overload and further accumulated when autophagy was inhibited with MRT, compared to the RAPA treatment (Fig. 7D-F). When autophagic flux was blocked using MRT and Baf-A, Fabp2 aggregated in SHK-1 cells under lipid overload, though to a lesser visual extent than Elovl6.

Based on these findings, we hypothesized that Elovl6 and Fabp2 are targets for autophagosomes. To provide further evidence of its targeting by autophagy, we asked whether Atlantic salmon Elovl6 and Fabp2 proteins have a LC3-interacting region motif (LIR motif). The LIR motif is a short linear sequence that facilitates the interaction between autophagy receptors and LC3 or other ATG8 family proteins [55]. The canonical LIR motif is characterized by a specific sequence pattern: Θ0-X1-X2-Γ3, where: 'Θ' (Theta) represents an aromatic residue, which can be tryptophan (W), phenylalanine (F), or tyrosine (Y). This residue is critical for the interaction with the hydrophobic pocket of LC3 or ATG8 proteins. 'X' represents any amino acid (aa), 'Γ' (Gamma) denotes an aliphatic residue, which can be leucine (L), valine (V), or isoleucine (I). This residue helps stabilize the interaction by binding to a different hydrophobic pocket of the LIR docking site. The arrangement of these residues enables the LIR motif to bind to the hydrophobic pockets of LC3 or ATG8 family proteins, promoting the recruitment of autophagy receptors to sites of autophagosome formation and facilitating autophagic degradation of the target protein [56].

As mentioned, the Atlantic salmon genome contains many co-orthologues of mammalian genes, owing to a history of fish-specific

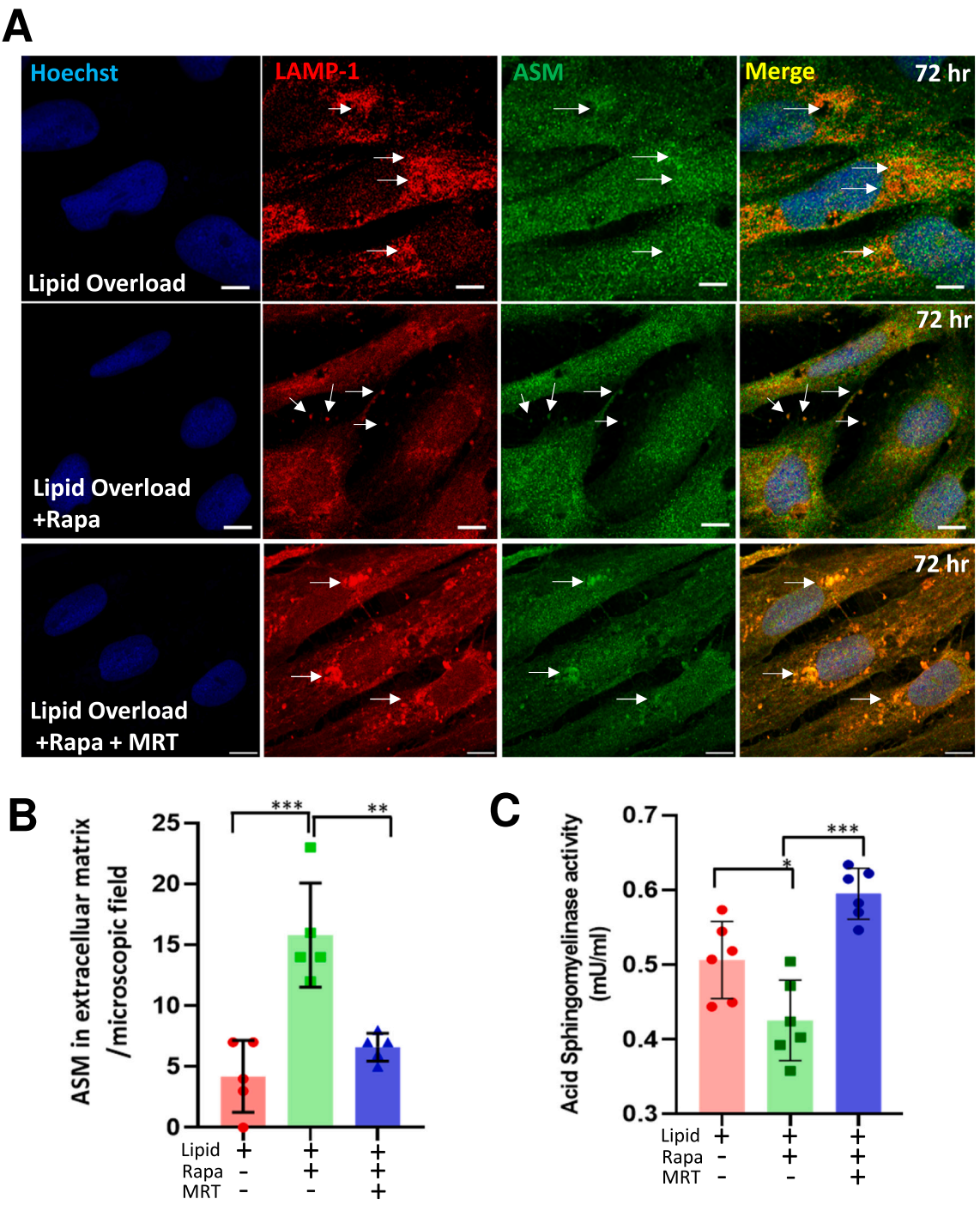

Fig. 5. Autophagy regulates ASM localization and modulates SMase activity. A. Representative confocal images showing the localisation of ASM (green) with LAMP-1 (red) in SHK-1 cells following 72 h treatment with lipid overload, lipid overload with RAPA and lipid overload with RAPA and MRT treatments. Scale bar = 5 μm, $n = 3$. B. Quantification of extracellular localisation of ASM with LAMP-1 positive vesicles (5–6 microscopic fields with minimum 9–10 cells each were used from 3 independent experiments). C. Evaluation of Acid SMase activity using fluorimetric assay ($n = 6$). Data shown are mean +/− SD, * $p < 0.05$; ** $p < 0.01$; *** $p < 0.001$. (For interpretation of the references to colour in this figure legend, the reader is referred to the web version of this article.)

whole genome duplication events during evolution [12]. Consistently, we identified five Elovl6 paralogues and four Fabp2 paralogues annotated in the NCBI Atlantic salmon genome (Ssal_v3.1, GCA_905237065.2), each encoding products sharing extensive homology with human Elovl6 and Fabp2. Note these annotations were consistent with genes identified in the Ensembl Ssal_v3.1 annotation (Supplementary Data 3). All these Atlantic salmon proteins were checked for a LIR motif using the iLIR Autophagy database [55] (Supplementary data 3). Each Elovl6 protein showed at least one xLIR motif (PSSM score of 10 or 11) and several WxxL motifs (PSSM score ranging from 1 to 9). One of the paralogues (ENSSSAG00000055568) showed evidence for two xLIR motifs with a PSSM score of 10 and 11 ($p < 0.001$)

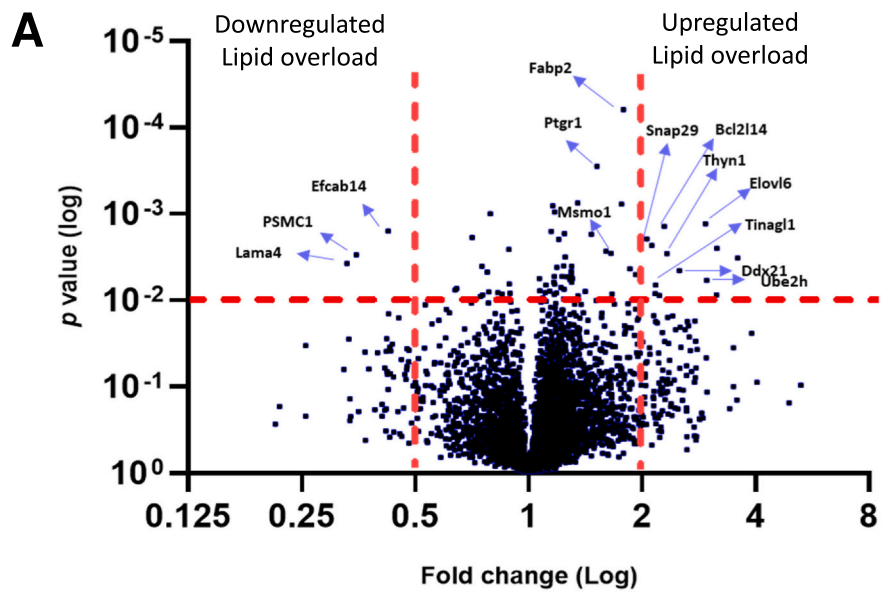

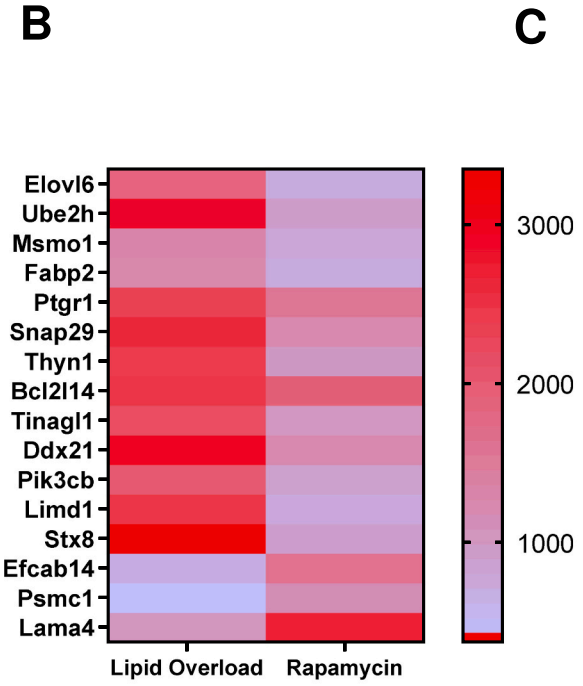

C

Protein Symbol	-log10 (*p*-value)
Elovl6	2.45757
Ube2h	2.42508
Msmo1	2.48512
Fabp2	2.34266
Ptgr1	1.99934
Snap29	1.92768
Thyn1	1.82324
Bcl2l14	1.65336
Tinagl1	1.63384
Ddx21	1.62445
Pik3cb	1.23392
Limd1	1.15865
Stx8	1.08904
Efcab14	0
PSMC1	1.79044
Lama4	1.55637

Fig. 6. Rapamycin ameliorates lipid overload mediated lipotoxicity. SHK-1 cells with lipid overload or lipid overload with RAPA treatment were analysed for proteome changes (72 h post-treatments). A. Volcano plot highlighting key protein targets among total 5971 proteins identified. B. Heat map of proteins showing abundance changes in the lipid overload treatment with <0.5-fold change or > 2-fold change ($p < 0.01$). C. Standardized value scores (log10 *p*-value) to represent the relative strength of the functional association of key protein targets with fatty liver (scores obtained from CTD Gene-Disease Associations dataset [81]).

and several WxxL motifs (Supplementary data 3). None of these motifs were present in the anchor region. Fabp2 proteins showed WxxL motifs (PSSM score ranging from 6 to 9). Interestingly, a LIR motif in the anchor was detected in Fabp2 paralogue ENSSSAG00000002671 (i.e., which showed increased protein abundance under lipid overload), which might suggest the presence of a functional LIR motif (Supplementary data 3).

These findings suggest that Atlantic salmon Elovl6 and Fabp2 proteins contain the expected motif to be targeted by selective autophagy.

3.6. mRNA expression of elovl6 and fabp2 genes remains largely unchanged under lipid overload and further RAPA treatment

Fig. 7A-B and D-E evidence an increase in intensity for Elovl6 and

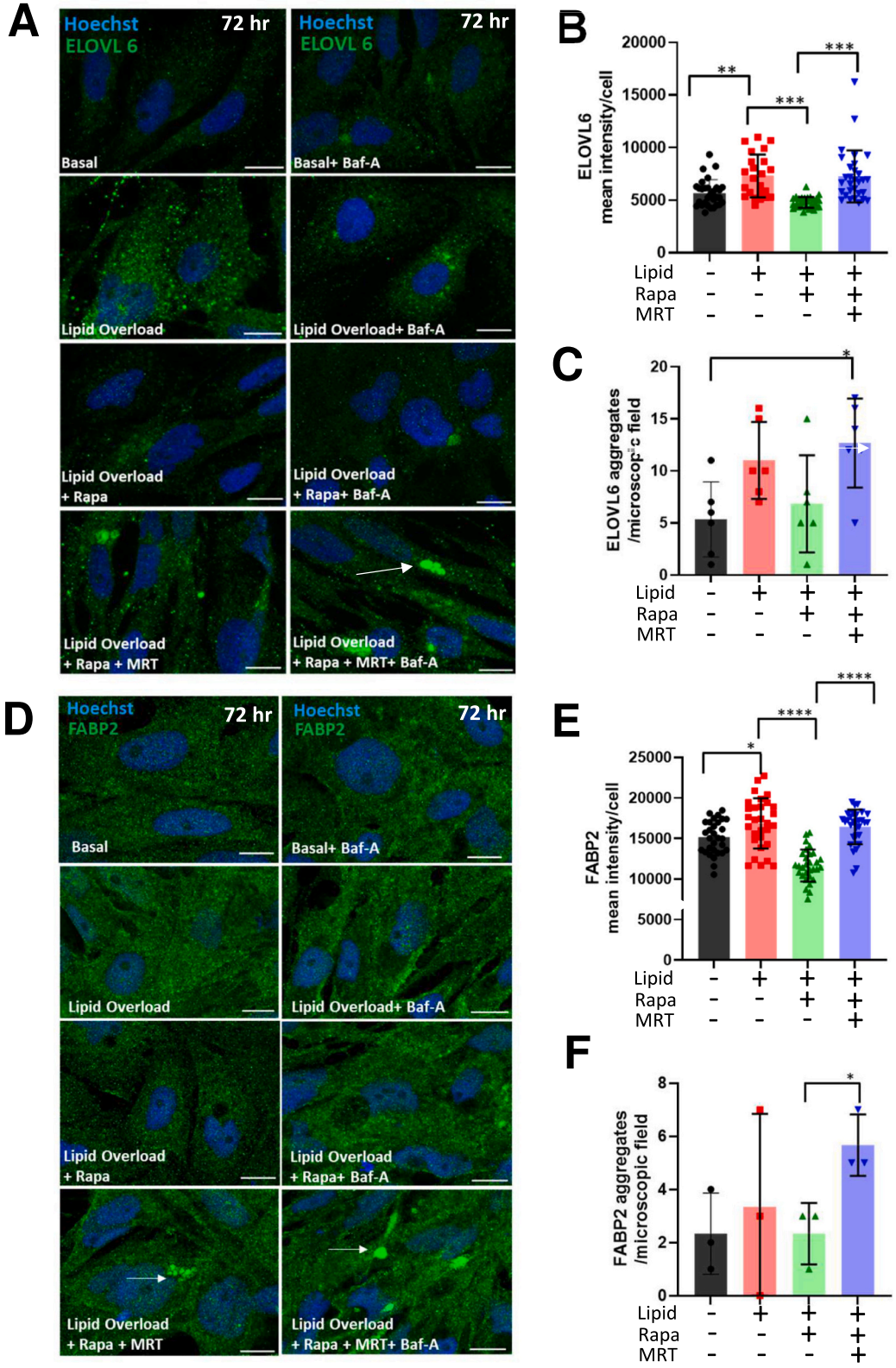

Fig. 7. Elovl6 and Fabp2 are possible target for autophagosomes. Representative confocal images showing expression of Elvol6 and Fabp2 in SHK-1 cells after 72 h treatment with no lipid overload, lipid overload, lipid overload with RAPA, and lipid overload with RAPA and MRT treatments, with and without Baf-A treatment to block autophagic flux. A-B. Increased expression of Elovl6 in lipid treated cells and its quantification (3 microscopic fields with minimum 9–10 cells each were used from 3 independent experiments). A and C Increased aggregation of Elovl6 on inhibition of autophagic flux with MRT and Baf-A (3 microscopic fields with minimum 9–10 cells each were used from 3 independent experiments). Scale bar = 10 μm, $n = 3$. White arrows indicate Elovl6 aggregations.
D-E. Increased expression of Fabp2 in lipid treated cells and its quantification (3 microscopic fields with minimum 9–10 cells each were used from 3 independent experiments). D and F Increased aggregation of Fabp2 on inhibition of autophagic flux with MRT and Baf-A (3 microscopic fields with minimum 9–10 cells each were used from 3 independent experiments). Scale bar = 10 μm, n = 3. White arrows indicate Fabp2 aggregations. Data shown are mean +/− SD, * $p < 0.05$; **** $p < 0.0001$.

Fabp2 proteins following lipid overload treatment, with a subsequent decrease on further RAPA treatment. This result was consistent with proteomic differences observed for the same target proteins contrasting the lipid overload and lipid overload + RAPA treatments (Fig. 6B). We next asked whether these changes can be explained by mRNA-level processes using qPCR. The two genes encoding Elovl6 (ENSSSAG00000074658) and Fabp2 (ENSSSAG00000002671) proteins showing strong differences according to proteomics showed no significant change in mRNA expression following lipid overload or further treatments with RAPA (Supplementary Fig. 4). This result suggests the observed protein-level changes do not result from regulation at the mRNA level; this makes sense for the inferred reduction of Elovl6 and Fabp2 protein following RAPA treatments, considering the evidence presented for autophagic degradation, such as the aggregation of these proteins when autophagy was blocked (Fig. 7). To be comprehensive in our approach, we also studied the expression of all identified *elovl6* and *fabp2* paralogues in the Atlantic salmon genome. This identified no changes in any *fabp2* gene, and evidence for mRNA upregulation of two *elovl6* paralogues (ENSSSAG00000055568 and ENSSSAG00000104628).

4. Discussion

Lipid recycling by autophagy, also known as lipophagy, has been extensively studied in mammals, where it plays crucial roles in LD turnover in hepatocytes [57] and adipocytes [58]. In *Drosophila*, which shares its core lipid metabolism pathways with vertebrates, small GTPase Rab40 is required for mobilisation of lipids via lipophagy [59]. Furthermore, RAPA treatment enhances lipophagy to prevents photoreceptor degeneration by blocking the formation of dihydroceramide, a precursor to CER accumulation in the *Drosophila* eye [60]. Lipophagy also plays important roles in lipid metabolism in zebrafish (*Danio rerio*) [3,61], where the simultaneous inhibition of cytosolic lipolysis and lipophagy resulted in severe liver damage with inflammation and damaged mitochondria [62]. Until this study, the role of lipophagy in Atlantic salmon has remained uncharacterised, an important knowledge gap considering the potentially key role that lipid homeostasis plays in the health of farmed fish. Using SHK-1 cells, we established a lipid overload model to investigate both lipotoxicity and lipid recycling by autophagy. This in vitro system offers flexibility for testing various autophagy inducers and inhibitors in a time and dose-dependent manner, while avoiding the use of live fish - aligning with principles of the 3Rs (Replacement, Reduction, and Refinement) in research [63].

Our experiments demonstrate reduced autophagic flux in Atlantic salmon SHK-1 cells under lipid overload, as indicated by the increased expression of SQSTM-1/p62 (Fig. 2). Additionally, a lipid overload treatment led to no significant change in LC3-I to LC3-II conversion following Baf-A treatment, suggesting a blockage in autophagic flux (Fig. 2). This parallels findings in vascular smooth muscle cells treated with saturated fatty acids, where a similar block in autophagic flux contributes to lipotoxicity [64]. We also observed accumulation of large LDs lacking Plin3 co-localisation and reduced protein levels of the two key lipase enzymes under lipid overload (Fig. 3), further suggesting inhibition of LD breakdown both by autophagy and cytosolic lipases. We observed a change in mitochondrial morphology, mitochondrial-LD interactions along with reduced mitochondrial potential under lipid overload (Supplementary Fig. 2). These observations will require further experiments to establish how mitochondrial-LD interactions effect energy homeostasis, specifically in terms of lipid biogenesis and mitochondrial β-oxidation.

Lipidomics under lipid overload conditions revealed an upregulation of several saturated SMs and CERs (Fig. 4), the key lipotoxic molecules implicated in various metabolic disorders [22,65]. De novo CER synthesis, fuelled by saturated fatty acids like palmitic acid [66] contributes to lipotoxicity by accumulating in LDs [67]. Additionally, SMs are converted to CERs by ASMs [68]. Our analysis pinpointed ASM as a key enzyme that co-localized with lysosomes under lipid overload, suggesting it represented lysosomal ASM, with a concomitant increase in ASM activity (Fig. 5). Proteomics also showed an upregulation (>2-fold) of proteins associated with fatty liver; a condition manifested by lipotoxicity (Fig. 6). Importantly, our experiments reveal that this lipotoxicity is effectively suppressed by enhancing autophagy. RAPA treatment not only reduced the accumulation of lipotoxic molecules, but also restored autophagic flux, evidenced by decreased SQSTM-1/p62 levels, enhanced LC3-I to LC3-II conversion, and a reduction in the number and size of LDs. Reduction in the number of LDs by RAPA treatment has elsewhere been demonstrated in palmitic acid induced foam cells [69].

Furthermore, RAPA treatment resulted in the accumulation of highly unsaturated TAGs, as indicated by the presence of multiple double bonds, which have a protective role against lipotoxicity induced by saturated fatty acids [70,71]. Based on the high number of double bonds observed in the high-carbon TAGs, we hypothesize that these TAGs are enriched in omega-3 fatty acids, which will require further experiments to test. Within the bounds of this study, attempts at measuring omega-3 levels using ELISA were unsuccessful, presumably due to the very low levels of DHA in SHK-1 cells (data not shown). This highlights the need for alternative methods or optimization of the assay to accurately measure omega-3 fatty acids in SHK-1 cells. Interestingly, RAPA-induced accumulation of TAGs has also been reported in microalgae, albeit with limited information on carbon chain length and the number of double bonds involved [72]. Enhanced accumulation of PUFA-TAGs by RAPA is possibly a protective mechanism against toxicity caused by reactive species produced by oxidation of membranous TAGs and associated increase in reactive oxygen species [71].

It is also worth noting that RAPA treatment resulted in exocytosis of ASM in LAMP-1 positive vesicles if SHK-1 cells. This secretory form of ASM plays a role in plasma membrane repair when cells are wounded in the presence of elevated calcium ions [73,74]. While, we did not measure calcium ion concentration in our treatments, enhanced calcium levels have been reported in the serum of patients with dysregulated lipid profiles [75].

By blocking the formation of autophagosomes using MRT, we further strengthened our claim that the suppression of lipotoxicity is indeed autophagy-dependent in SHK-1 cells. Blocking autophagic flux with MRT resulted in a significant increase in LD size, ASM localisation to the lysosomes and an increase in Elovl6 aggregation, supporting the hypothesis that autophagy is required to regulate the lipotoxic environment. This further suggests that the autophagy pathway is crucial in mitigating lipotoxic effects by managing lipid storage and degradation processes.

In humans and mice, autophagy levels decline with age, which also increases susceptibility to lipotoxicity [76–80]. However, such data is not yet available for farmed Atlantic salmon in vivo. Our findings suggest that enhancing autophagy in salmon cells can restore lipid homeostasis, potentially presenting a promising approach to counteracting lipotoxicity induced by dietary factors (i.e., increased vegetable oils in farmed fish diets) or a sedentary domesticated lifestyle, particularly as the fish age during aquaculture production. However, because the findings of this study are restricted to in vitro experiments, they firstly need to be validated in vivo following autophagy induction in live fish. Assuming similar results are obtained in vivo, dietary supplementation to activate autophagy could offer a novel strategy to produce healthier fish with improved lipid profiles, which in turn may lead to increased robustness in salmon aquaculture. As another obvious next step, our results should be validated using alternative autophagy inducers, especially those amenable for use as in vivo feed supplements on large fish during the final stage of production leading to harvest.

Supplementary data to this article can be found online at https://doi.org/10.1016/j.bbalip.2025.159636.

CRediT authorship contribution statement

Kanchan Phadwal: Writing – original draft, Validation, Methodology, Investigation, Funding acquisition, Formal analysis, Conceptualization. **Jennifer Haggarty:** Writing – review & editing, Methodology, Formal analysis, Data curation. **Dominic Kurian:** Writing – review & editing, Formal analysis, Data curation. **Judit Aguilar Martí:** Writing – review & editing, Software, Methodology, Investigation, Formal analysis, Data curation. **Jianxuan Sun:** Software, Methodology. **Ross D. Houston:** Writing – review & editing, Conceptualization. **Mónica B. Betancor:** Writing – review & editing. **Vicky E. MacRae:** Writing – review & editing, Supervision, Funding acquisition. **Phillip D. Whitfield:** Writing – review & editing, Methodology, Formal analysis, Data curation. **Daniel J. Macqueen:** Writing – review & editing, Writing – original draft, Supervision, Project administration, Funding acquisition.

Funding sources

This work was supported by funding from the Scottish Universities Life Sciences Alliance (SULSA ECR Development funding to K.P.), the BBSRC (Roslin Institute pump priming grant to K.P. and Institute Strategic Programme grants BB/J004316/1; BBS/E/RL/230001C and BBS/E/D/10002071) and the Seafood innovation fund (grant RD204 to K.P.).

Declaration of competing interest

The authors declare the following financial interests/personal relationships which may be considered as potential competing interests: Kanchan Phadwal reports financial support was provided by UK Sea Food Innovation Fund. No Conflict of Interest If there are other authors, they declare that they have no known competing financial interests or personal relationships that could have appeared to influence the work reported in this paper.

Acknowledgements

We thank Dr. Anna Raper (Bioimaging Facility Manager, Roslin Institute) for support with the immunofluorescence experiments. We thank, Dr. Ye Hwa Jin and Dr. Diego Robledo from The Roslin Institute for their help with SHK-1 cell culture. We thank the Cellular Analysis Facility at University of Glasgow for their support & assistance in this work.

Data availability

All data referenced in the manuscript are included as supplementary files. The raw proteomics data will be submitted to the PRIDE repository.

References

[1] Y. Aman, T. Schmauck-Medina, M. Hansen, R.I. Morimoto, A.K. Simon, I. Bjedov, K. Palikaras, A. Simonsen, T. Johansen, N. Tavernarakis, D.C. Rubinsztein, L. Partridge, G. Kroemer, J. Labbadia, E.F. Fang, Autophagy in healthy aging and disease, Nat. Aging 1 (2021) 634–650.

[2] Z. Yang, D.J. Klionsky, An overview of the molecular mechanism of autophagy, Curr. Top. Microbiol. Immunol. 335 (2009) 1–32.

[3] S. Zhang, X. Peng, S. Yang, X. Li, M. Huang, S. Wei, J. Liu, G. He, H. Zheng, L. Yang, H. Li, Q. Fan, The regulation, function, and role of lipophagy, a form of selective autophagy, in metabolic disorders, Cell Death Dis. 13 (2022) 132.

[4] T.B. Nguyen, J.A. Olzmann, Lipid droplets and lipotoxicity during autophagy, Autophagy 13 (2017) 2002–2003.

[5] S. Sarkar, B. Carroll, Y. Buganim, D. Maetzel, A.H. Ng, J.P. Cassady, M.A. Cohen, S. Chakraborty, H. Wang, E. Spooner, H. Ploegh, J. Gsponer, V.I. Korolchuk, R. Jaenisch, Impaired autophagy in the lipid-storage disorder Niemann-Pick type C1 disease, Cell Rep. 5 (2013) 1302–1315.

[6] T.B. Nguyen, S.M. Louie, J.R. Daniele, Q. Tran, A. Dillin, R. Zoncu, D.K. Nomura, J. A. Olzmann, DGAT1-dependent lipid droplet biogenesis protects mitochondrial function during starvation-induced autophagy, Dev. Cell 42 (2017), 9-21 e25.

[7] C. Preuss, T. Jelenik, K. Bodis, K. Mussig, V. Burkart, J. Szendroedi, M. Roden, D. F. Markgraf, A new targeted lipidomics approach reveals lipid droplets in liver, muscle and heart as a repository for diacylglycerol and ceramide species in non-alcoholic fatty liver, Cells 8 (3) (2019) 277, https://doi.org/10.3390/cells8030277.

[8] T.D. Mullen, Y.A. Hannun, L.M. Obeid, Ceramide synthases at the centre of sphingolipid metabolism and biology, Biochem. J. 441 (2012) 789–802.

[9] M. Brankovic, I. Jovanovic, M. Dukic, T. Radonjic, S. Opric, S. Klasnja, M. Zdravkovic, Lipotoxicity as the leading cause of non-alcoholic steatohepatitis, Int. J. Mol. Sci. 23 (2022).

[10] M. Nakamura, Lipotoxicity as a therapeutic target in obesity and diabetic cardiomyopathy, J. Pharm. Pharm. Sci. 27 (2024) 12568.

[11] A. Brun, P. Denis, M. Rambeau, J.P. Rigaudiere, C. Jouve, V. Mazurak, F. Capel, Polyunsaturated fatty acids prevent myosteatosis and lipotoxicity, J. Nutr. Biochem. 134 (2024) 109722, https://doi.org/10.1016/j.jnutbio.2024.109722.

[12] R.D. Houston, D.J. Macqueen, Atlantic salmon (Salmo salar L.) genetics in the 21st century: taking leaps forward in aquaculture and biological understanding, Anim. Genet. 50 (2019) 3–14.

[13] R.L. Naylor, R.W. Hardy, A.H. Buschmann, S.R. Bush, L. Cao, D.H. Klinger, D. C. Little, J. Lubchenco, S.E. Shumway, M. Troell, A 20-year retrospective review of global aquaculture, Nature 591 (2021) 551–563.

[14] B. Zlaugotne, J. Pubule, D. Blumberga, Advantages and disadvantages of using more sustainable ingredients in fish feed, Heliyon 8 (2022) e10527.

[15] B.E. Torstensen, M. Espe, I. Stubhaug, O. Lie, Dietary plant proteins and vegetable oil blends increase adiposity and plasma lipids in Atlantic salmon (Salmo salar L.), Br. J. Nutr. 106 (2011) 633–647.

[16] J.G. Bell, J.R. Dick, A.H. McVicar, J.R. Sargent, K.D. Thompson, Dietary sunflower, linseed and fish oils affect phospholipid fatty acid composition, development of cardiac lesions, phospholipase activity and eicosanoid production in Atlantic salmon (Salmo salar), Prostaglandins Leukot. Essent. Fatty Acids 49 (1993) 665–673.

[17] A.R. Alvheim, B.E. Torstensen, Y.H. Lin, H.H. Lillefosse, E.J. Lock, L. Madsen, L. Froyland, J.R. Hibbeln, M.K. Malde, Dietary linoleic acid elevates the endocannabinoids 2-AG and anandamide and promotes weight gain in mice fed a low fat diet, Lipids 49 (2014) 59–69.

[18] A.R. Alvheim, B.E. Torstensen, Y.H. Lin, H.H. Lillefosse, E.J. Lock, L. Madsen, J. R. Hibbeln, M.K. Malde, Dietary linoleic acid elevates endogenous 2-arachidonoylglycerol and anandamide in Atlantic salmon (Salmo salar L.) and mice, and induces weight gain and inflammation in mice, Br. J. Nutr. 109 (2013) 1508–1517.

[19] L.K. Midtbo, A.G. Borkowska, A. Bernhard, A.K. Ronnevik, E.J. Lock, M. L. Fitzgerald, B.E. Torstensen, B. Liaset, T. Brattelid, T.L. Pedersen, J.W. Newman, K. Kristiansen, L. Madsen, Intake of farmed Atlantic salmon fed soybean oil increases hepatic levels of arachidonic acid-derived oxylipins and ceramides in mice, J. Nutr. Biochem. 26 (2015) 585–595.

[20] L.K. Midtbo, M.M. Ibrahim, L.S. Myrmel, U.L. Aune, A.R. Alvheim, N.S. Liland, B. E. Torstensen, G. Rosenlund, B. Liaset, T. Brattelid, K. Kristiansen, L. Madsen, Intake of farmed Atlantic salmon fed soybean oil increases insulin resistance and hepatic lipid accumulation in mice, PloS One 8 (2013) e53094.

[21] M. Misheva, J. Johnson, J. McCullagh, Role of oxylipins in the inflammatory-related diseases NAFLD, obesity, and type 2 diabetes, Metabolites 12 (2022).

[22] B. Chaurasia, S.A. Summers, Ceramides-lipotoxic inducers of metabolic disorders, Trends Endocrinol. Metab. 26 (2015) 538–550.

[23] B.H. Dannevig, K. Falk, E. Namork, Isolation of the causal virus of infectious salmon anaemia (ISA) in a long-term cell line from Atlantic salmon head kidney, J. Gen. Virol. 76 (Pt 6) (1995) 1353–1359.

[24] S. Beyaz, M.D. Mana, J. Roper, D. Kedrin, A. Saadatpour, S.J. Hong, K.E. Bauer-Rowe, M.E. Xifaras, A. Akkad, E. Arias, L. Pinello, Y. Katz, S. Shinagare, M. Abu-Remaileh, M.M. Mihaylova, D.W. Lamming, R. Dogum, G. Guo, G.W. Bell, M. Selig, G.P. Nielsen, N. Gupta, C.R. Ferrone, V. Deshpande, G.C. Yuan, S.H. Orkin, D. M. Sabatini, O.H. Yilmaz, High-fat diet enhances stemness and tumorigenicity of intestinal progenitors, Nature 531 (2016) 53–58.

[25] J. Schindelin, I. Arganda-Carreras, E. Frise, V. Kaynig, M. Longair, T. Pietzsch, S. Preibisch, C. Rueden, S. Saalfeld, B. Schmid, J.Y. Tinevez, D.J. White, V. Hartenstein, K. Eliceiri, P. Tomancak, A. Cardona, Fiji: an open-source platform for biological-image analysis, Nat. Methods 9 (2012) 676–682.

[26] A. Untergasser, I. Cutcutache, T. Koressaar, J. Ye, B.C. Faircloth, M. Remm, S. G. Rozen, Primer3–new capabilities and interfaces, Nucleic Acids Res. 40 (2012) e115.

[27] J. Folch, M. Lees, G.H. Sloane Stanley, A simple method for the isolation and purification of total lipides from animal tissues, J. Biol. Chem. 226 (1) (1957) 497–509, https://doi.org/10.1016/S0021-9258(18)64849-5.

[28] T.D. Rose, N. Kohler, L. Falk, L. Klischat, O.E. Lazareva, J.K. Pauling, Lipid network and moiety analysis for revealing enzymatic dysregulation and mechanistic alterations from lipidomics data, Brief. Bioinform. 24 (2023).

[29] J. Zhang, L. Xin, B. Shan, W. Chen, M. Xie, D. Yuen, W. Zhang, Z. Zhang, G. A. Lajoie, B. Ma, PEAKS DB: de novo sequencing assisted database search for sensitive and accurate peptide identification, Mol. Cell. Proteomics 11 (2012), https://doi.org/10.1074/mcp.M111.010587. M111 010587 4.

[30] M. Tanemura, Y. Ohmura, T. Deguchi, T. Machida, R. Tsukamoto, H. Wada, S. Kobayashi, S. Marubashi, H. Eguchi, T. Ito, H. Nagano, M. Mori, Y. Doki, Rapamycin causes upregulation of autophagy and impairs islets function both in vitro and in vivo, Am. J. Transplant. 12 (2012) 102–114.

[31] K.J. Petherick, O.J. Conway, C. Mpamhanga, S.A. Osborne, A. Kamal, B. Saxty, I. G. Ganley, Pharmacological inhibition of ULK1 kinase blocks mammalian target of rapamycin (mTOR)-dependent autophagy, J. Biol. Chem. 290 (2015) 28726.

[32] J. Zou, F. Yue, W. Li, K. Song, X. Jiang, J. Yi, L. Liu, Autophagy inhibitor LRPPRC suppresses mitophagy through interaction with mitophagy initiator Parkin, PloS One 9 (2014) e94903.

[33] C. Mauvezin, T.P. Neufeld, Bafilomycin A1 disrupts autophagic flux by inhibiting both V-ATPase-dependent acidification and Ca-P60A/SERCA-dependent autophagosome-lysosome fusion, Autophagy 11 (2015) 1437–1438.
[34] X. Sun, Q. Yu, Y. Qi, B. Kang, X. Zhao, L. Liu, P. Wang, M. Cong, T. Liu, Peridroplet mitochondria are associated with the severity of MASLD and the prevention of MASLD by diethyldithiocarbamate, J. Lipid Res. 65 (2024) 100590.
[35] L.W. Brier, L. Ge, G. Stjepanovic, A.M. Thelen, J.H. Hurley, R. Schekman, Regulation of LC3 lipidation by the autophagy-specific class III phosphatidylinositol-3 kinase complex, Mol. Biol. Cell 30 (2019) 1098–1107.
[36] S.R. Yoshii, N. Mizushima, Monitoring and measuring autophagy, Int. J. Mol. Sci. 18 (2017).
[37] M. Garcia-Macia, A. Santos-Ledo, J. Leslie, H.L. Paish, A.L. Collins, R.S. Scott, A. Watson, R.A. Burgoyne, S. White, J. French, J. Hammond, L.A. Borthwick, J. Mann, J.P. Bolanos, V.I. Korolchuk, F. Oakley, D.A. Mann, A mammalian target of rapamycin-Perilipin 3 (mTORC1-Plin3) pathway is essential to activate lipophagy and protects against hepatosteatosis, Hepatology 74 (2021) 3441–3459.
[38] E. Smirnova, E.B. Goldberg, K.S. Makarova, L. Lin, W.J. Brown, C.L. Jackson, ATGL has a key role in lipid droplet/adiposome degradation in mammalian cells, EMBO Rep. 7 (2006) 106–113.
[39] D.W. Shin, Lipophagy: molecular mechanisms and implications in metabolic disorders, Mol. Cells 43 (2020) 686–693.
[40] H. Hanamatsu, S. Ohnishi, S. Sakai, K. Yuyama, S. Mitsutake, H. Takeda, S. Hashino, Y. Igarashi, Altered levels of serum sphingomyelin and ceramide containing distinct acyl chains in young obese adults, Nutr. Diabetes 4 (2014) e141.
[41] B.D. McNally, D.F. Ashley, L. Hanschke, H.N. Daou, N.T. Watt, S.A. Murfitt, A.D. V. MacCannell, A. Whitehead, T.S. Bowen, F.W.B. Sanders, M. Vacca, K.K. Witte, G. R. Davies, R. Bauer, J.L. Griffin, L.D. Roberts, Long-chain ceramides are cell non-autonomous signals linking lipotoxicity to endoplasmic reticulum stress in skeletal muscle, Nat. Commun. 13 (2022) 1748.
[42] A. Akoumi, T. Haffar, M. Mousterji, R.S. Kiss, N. Bousette, Palmitate mediated diacylglycerol accumulation causes endoplasmic reticulum stress, Plin2 degradation, and cell death in H9C2 cardiomyoblasts, Exp. Cell Res. 354 (2017) 85–94.
[43] J.P. Mann, B. Jenkins, S. Furse, S.G. Snowden, A. Alisi, L.G. Draijer, K. Karnebeek, D.A. Kelly, B.G. Koot, A. Mosca, C. Salvestrini, I. van Mourik, A. Vreugdenhil, M. Zilbauer, A. Koulman, E.-P. investigators, Comparison of the lipidomic signature of fatty liver in children and adults: a cross-sectional study, J. Pediatr. Gastroenterol. Nutr. 74 (2022) 734–741.
[44] A.J. McGlinchey, O. Govaere, D. Geng, V. Ratziu, M. Allison, J. Bousier, S. Petta, C. de Oliviera, E. Bugianesi, J.M. Schattenberg, A.K. Daly, T. Hyotylainen, Q. M. Anstee, M. Oresic, Metabolic signatures across the full spectrum of non-alcoholic fatty liver disease, JHEP Rep. 4 (2022) 100477.
[45] E.B. Yalcin, M. Tong, K. Cao, C.K. Huang, S. de la Monte, High fat diet mediated alterations in serum sphingolipid profiles in an experimental mouse model measured by matrix-assisted laser desorption/ionization-time of flight mass spectrometry, Eur. J. Biol. Biotechnol. 4 (2023) 25–32.
[46] B. Breiden, K. Sandhoff, Acid sphingomyelinase, a lysosomal and secretory phospholipase C, is key for cellular phospholipid catabolism, Int. J. Mol. Sci. 22 (2021).
[47] J.K. Lee, H.K. Jin, M.H. Park, B.R. Kim, P.H. Lee, H. Nakauchi, J.E. Carter, X. He, E. H. Schuchman, J.S. Bae, Acid sphingomyelinase modulates the autophagic process by controlling lysosomal biogenesis in Alzheimer's disease, J. Exp. Med. 211 (2014) 1551–1570.
[48] X. Li, M. Xu, A.L. Pitzer, M. Xia, K.M. Boini, P.L. Li, Y. Zhang, Control of autophagy maturation by acid sphingomyelinase in mouse coronary arterial smooth muscle cells: protective role in atherosclerosis, J. Mol. Med. (Berl) 92 (2014) 473–485.
[49] R. Fucho, L. Martinez, A. Baulies, S. Torres, N. Tarrats, A. Fernandez, V. Ribas, A. M. Astudillo, J. Balsinde, P. Garcia-Roves, M. Elena, I. Bergheim, S. Lotersztajn, C. Trautwein, H. Appelqvist, A.W. Paton, J.C. Paton, M.J. Czaja, N. Kaplowitz, J. C. Fernandez-Checa, C. Garcia-Ruiz, ASMase regulates autophagy and lysosomal membrane permeabilization and its inhibition prevents early stage non-alcoholic steatohepatitis, J. Hepatol. 61 (2014) 1126–1134.
[50] A.D. Rouillard, G.W. Gundersen, N.F. Fernandez, Z. Wang, C.D. Monteiro, M. G. McDermott, A. Ma'ayan, The harmonizome: a collection of processed datasets gathered to serve and mine knowledge about genes and proteins, Database (Oxford) (2016) 2016.
[51] T. Matsuzaka, H. Shimano, Elovl6: a new player in fatty acid metabolism and insulin sensitivity, J. Mol. Med. (Berl) 87 (2009) 379–384.
[52] T. Matsuzaka, A. Atsumi, R. Matsumori, T. Nie, H. Shinozaki, N. Suzuki-Kemuriyama, M. Kuba, Y. Nakagawa, K. Ishii, M. Shimada, K. Kobayashi, S. Yatoh, A. Takahashi, K. Takekoshi, H. Sone, N. Yahagi, H. Suzuki, S. Murata, M. Nakamuta, N. Yamada, H. Shimano, Elovl6 promotes nonalcoholic steatohepatitis, Hepatology 56 (2012) 2199–2208.
[53] M. Andre, S. Ando, C. Ballagny, M. Durliat, G. Poupard, C. Briancon, P.J. Babin, Intestinal fatty acid binding protein gene expression reveals the cephalocaudal patterning during zebrafish gut morphogenesis, Int. J. Dev. Biol. 44 (2000) 249–252.
[54] Y. Zhang, X. Cao, J. Gao, Cloning of fatty acid-binding protein 2 (fabp2) in loach (Misgurnus anguillicaudatus) and its expression in response to dietary oxidized fish oil, Comp. Biochem. Physiol. B Biochem. Mol. Biol. 229 (2019) 26–33.
[55] A.C. Jacomin, S. Samavedam, V. Promponas, I.P. Nezis, iLIR database: a web resource for LIR motif-containing proteins in eukaryotes, Autophagy 12 (2016) 1945–1953.
[56] T. Johansen, T. Lamark, Selective autophagy: ATG8 family proteins, LIR motifs and cargo receptors, J. Mol. Biol. 432 (2020) 80–103.
[57] Y. Minami, A. Hoshino, Y. Higuchi, M. Hamaguchi, Y. Kaneko, Y. Kirita, S. Taminishi, T. Nishiji, A. Taruno, M. Fukui, Z. Arany, S. Matoba, Liver lipophagy ameliorates nonalcoholic steatohepatitis through extracellular lipid secretion, Nat. Commun. 14 (2023) 4084.
[58] D. Lettieri Barbato, G. Tatulli, K. Aquilano, M.R. Ciriolo, FoxO1 controls lysosomal acid lipase in adipocytes: implication of lipophagy during nutrient restriction and metformin treatment, Cell Death Dis. 4 (2013) e861.
[59] X. Duan, L. Xu, Y. Li, L. Jia, W. Liu, W. Shao, V. Bayat, W. Shang, L. Wang, J.P. Liu, C. Tong, Regulation of lipid homeostasis by the TBC protein dTBC1D22 via modulation of the small GTPase Rab40 to facilitate lipophagy, Cell Rep. 36 (2021) 109541.
[60] W.H. Jung, C.C. Liu, Y.L. Yu, Y.C. Chang, W.Y. Lien, H.C. Chao, S.Y. Huang, C. H. Kuo, H.C. Ho, C.C. Chan, Lipophagy prevents activity-dependent neurodegeneration due to dihydroceramide accumulation in vivo, EMBO Rep. 18 (2017) 1150–1165.
[61] J. Wang, S.L. Han, D.L. Lu, L.Y. Li, S.M. Limbu, D.L. Li, M.L. Zhang, Z.Y. Du, Inhibited lipophagy suppresses lipid metabolism in zebrafish liver cells, Front. Physiol. 10 (1077) (2019) 1077, https://doi.org/10.3389/fphys.2019.01077.
[62] S.L. Han, Y.C. Qian, S.M. Limbu, J. Wang, L.Q. Chen, M.L. Zhang, Z.Y. Du, Lipolysis and lipophagy play individual and interactive roles in regulating triacylglycerol and cholesterol homeostasis and mitochondrial form in zebrafish, Biochim. Biophys. Acta Mol. Cell Biol. Lipids 1866 (2021) 158988.
[63] P. Flecknell, Replacement, reduction and refinement, ALTEX 19 (2002) 73–78.
[64] Y. Shiozaki, S. Miyazaki-Anzai, K. Okamura, A.L. Keenan, M. Masuda, M. Miyazaki, GPAT4-generated saturated LPAs induce lipotoxicity through inhibition of autophagy by abnormal formation of omegasomes, IScience 23 (2020) 101105.
[65] C.L. Bandet, S. Tan-Chen, O. Bourron, H. Le Stunff, E. Hajduch, Sphingolipid metabolism: new insight into ceramide-induced lipotoxicity in muscle cells, Int. J. Mol. Sci. 20 (2019).
[66] L. Martinez, S. Torres, A. Baulies, C. Alarcon-Vila, M. Elena, G. Fabrias, J. Casas, J. Caballeria, J.C. Fernandez-Checa, C. Garcia-Ruiz, Myristic acid potentiates palmitic acid-induced lipotoxicity and steatohepatitis associated with lipodystrophy by sustaning de novo ceramide synthesis, Oncotarget 6 (2015) 41479–41496.
[67] C.E. Senkal, M.F. Salama, A.J. Snider, J.J. Allopenna, N.A. Rana, A. Koller, Y. A. Hannun, L.M. Obeid, Ceramide is metabolized to acylceramide and stored in lipid droplets, Cell Metab. 25 (2017) 686–697.
[68] I.H. Mir, C. Thirunavukkarasu, The relevance of acid sphingomyelinase as a potential target for therapeutic intervention in hepatic disorders: current scenario and anticipated trends, Arch. Toxicol. 97 (2023) 2069–2087.
[69] H. Zheng, Y. Fu, Y. Huang, X. Zheng, W. Yu, W. Wang, mTOR signaling promotes foam cell formation and inhibits foam cell egress through suppressing the SIRT1 signaling pathway, Mol. Med. Rep. 16 (2017) 3315–3323.
[70] C.J. Urso, H. Zhou, Palmitic acid lipotoxicity in microglia cells is ameliorated by unsaturated fatty acids, Int. J. Mol. Sci. 22 (2021).
[71] N. Li, Y. Sancak, J. Frasor, G.E. Atilla-Gokcumen, A protective role for triacylglycerols during apoptosis, Biochemistry 57 (2018) 72–80.
[72] S. Imamura, Y. Kawase, I. Kobayashi, M. Shimojima, H. Ohta, K. Tanaka, TOR (target of rapamycin) is a key regulator of triacylglycerol accumulation in microalgae, Plant Signal. Behav. 11 (2016) e1149285.
[73] C. Tam, V. Idone, C. Devlin, M.C. Fernandes, A. Flannery, X. He, E. Schuchman, I. Tabas, N.W. Andrews, Exocytosis of acid sphingomyelinase by wounded cells promotes endocytosis and plasma membrane repair, J. Cell Biol. 189 (2010) 1027–1038.
[74] N.W. Andrews, Solving the secretory acid sphingomyelinase puzzle: insights from lysosome-mediated parasite invasion and plasma membrane repair, Cell. Microbiol. 21 (11) (2019) e13065, https://doi.org/10.1111/cmi.13065.
[75] L. Gallo, M.C. Faniello, G. Canino, C. Tripolino, A. Gnasso, G. Cuda, F.S. Costanzo, C. Irace, Serum calcium increase correlates with worsening of lipid profile: an observational study on a large cohort from South Italy, Medicine (Baltimore) 95 (2016) e2774.
[76] K. Phadwal, J. Alegre-Abarrategui, A.S. Watson, L. Pike, S. Anbalagan, E. M. Hammond, R. Wade-Martins, A. McMichael, P. Klenerman, A.K. Simon, A novel method for autophagy detection in primary cells: impaired levels of macroautophagy in immunosenescent T cells, Autophagy 8 (2012) 677–689.
[77] A.M. Cuervo, A.V. Gomes, J.A. Barnes, J.F. Dice, Selective degradation of annexins by chaperone-mediated autophagy, J. Biol. Chem. 275 (2000) 33329–33335.
[78] M. Slawik, A.J. Vidal-Puig, Lipotoxicity, overnutrition and energy metabolism in aging, Ageing Res. Rev. 5 (2006) 144–164.
[79] W. Guo, T. Pirtskhalava, T. Tchkonia, W. Xie, T. Thomou, J. Han, T. Wang, S. Wong, A. Cartwright, F.G. Hegardt, B.E. Corkey, J.L. Kirkland, Aging results in paradoxical susceptibility of fat cell progenitors to lipotoxicity, Am. J. Physiol. Endocrinol. Metab. 292 (2007) E1041–E1051.
[80] A.J. Stranks, A.L. Hansen, I. Panse, M. Mortensen, D.J. Ferguson, D.J. Puleston, K. Shenderov, A.S. Watson, M. Veldhoen, K. Phadwal, V. Cerundolo, A.K. Simon, Autophagy controls acquisition of aging features in macrophages, J. Innate Immun. 7 (2015) 375–391.
[81] A.P. Davis, C.J. Grondin, K. Lennon-Hopkins, C. Saraceni-Richards, D. Sciaky, B. L. King, T.C. Wiegers, C.J. Mattingly, The comparative toxicogenomics database's 10th year anniversary: update 2015, Nucleic Acids Res. 43 (2015) D914–D920.